CM² MAGAZINE

第 51 期

南方科技大学海洋磁学中心主编

创刊词

海洋是生命的摇篮，是文明的纽带。地球上最早的生命诞生于海洋，海洋里的生命最终进化成了人类，人类的文化融合又通过海洋得以实现。人因海而兴。

人类对海洋的探索从未停止。从远古时代美丽的神话传说，到麦哲伦的全球航行，再到现代对大洋的科学钻探计划，海洋逐渐从人类敬畏崇拜幻想的精神寄托演变成可以开发利用与科学研究的客观存在。其中，上个世纪与太空探索同步发展的大洋科学钻探计划将人类对海洋的认知推向了崭新的纬度：深海（deep sea）与深时（deep time）。大洋钻探计划让人类知道，奔流不息的大海之下，埋藏的却是亿万年的地球历史。它们记录了地球板块的运动，从而使板块构造学说得到证实；它们记录了地球环境的演变，从而让古海洋学方兴未艾。

在探索海洋的悠久历史中，从大航海时代的导航，到大洋钻探计划中不可或缺的磁性地层学，磁学发挥了不可替代的作用。这不是偶然，因为从微观到宏观，磁性是最基本的物理属性之一，可以说，万物皆有磁性。基于课题组的学科背景和对海洋的理解，我们对海洋的探索以磁学为主要手段，海洋磁学中心因此而生。

海洋磁学中心，简称 CM^2，一为其全名“Centre for Marine Magnetism”的缩写，另者恰与爱因斯坦著名的质能方程 $E = MC^2$ 对称，借以表达我们对科学巨匠的敬仰和对科学的不懈追求。

然而科学从来不是单打独斗的产物。我们以磁学为研究海洋的主攻利器，但绝不仅限于磁学。凡与磁学相关的领域均是我们关注的重点。为了跟踪反映国内外地球科学特别是与磁学有关的地球科学领域的最新研究进展，海洋磁学中心特地主办 CM^2 Magazine，以期与各位地球科学工作者相互交流学习、合作共进！

“海洋孕育了生命，联通了世界，促进了发展”。 21 世纪是海洋科学的时代，由陆向海，让我们携手迈进中国海洋科学的黄金时代。

目 录

研究进展

李金华等，Journal of Geophysical Research: Biogeoscience：细菌利用地磁场上下穿梭驱动有氧-无氧界面物质和能量循环

趋磁细菌是一类能在细胞内合成纳米磁性晶体颗粒（也被称为磁小体，化学成分为 Fe_3O_4 或 Fe_3S_4）的原核生物。磁小体多呈链状排列，作为细胞的小磁针，可以感知地磁场，使其沿磁力线方向游泳，从而迅速找到最适合生存的微环境，即水体中“有氧-无氧界面（OAI）”。学界把这种行为称作“趋磁性”或“磁辅助-趋化性”。自上世纪六七十年代以来，趋磁细菌被作为理想的模式系统，被广泛用来研究生物地磁响应行为及其分子机制。长期以来，“趋磁性”或“磁辅助-趋化性”被认为是趋磁细菌受到地磁场的扭力作用，而被地磁场定向后，在鞭毛的推动下，向上或向下游动到水体中的 OAI 界面附近。

近日，中国科学院地质与地球物理研究所科学团队成员联合国内外多个单位科研人员，发现趋磁细菌利用地磁场的定向作用，在 OAI 中上下穿梭，从而将 OAI 上部有氧或微氧与其下部的厌氧环境联动起来，进而驱动碳、氮、硫和铁等在地球水生环境的无氧与有氧环境中的元素循环。相关研究成果发表在《Journal of Geophysical Research: Biogeoscience》上，并被选为 AGU 亮点文章（AGU Research Spotlight），并在其 EOS 网站进行了相关报道（https://eos.org/research-spotlights/chemical-shuttling-bacteria-follow-earths-magnetic-field），指示趋磁细菌可能是一类重要的微生物功能群，在地球水生环境的物质和能量循环中起重要作用。同时，该研究还提出了一种“细菌利用地磁场在水体有氧-无氧界面上下穿梭驱动微生物硫循环”的新机制。

OAI 是地球上有氧与无氧环境之间的过渡带。在地球的水生环境中（如海洋、湖泊、沼泽和河流），OAI 主要存在于沉积物表层或者具有化学梯度分层的水体中。氧气（O_2）与硫化氢（H_2S）的反向化学梯度变化是水生环境 OAI 的最重要特征。一般来讲，从上向下，氧气浓度逐渐降低；而从下向上，硫化氢浓度逐渐递减；中间通常还存在一个二者浓度极低或者都缺失的地带，其厚度变化很大，从几厘米到几十米都存在。

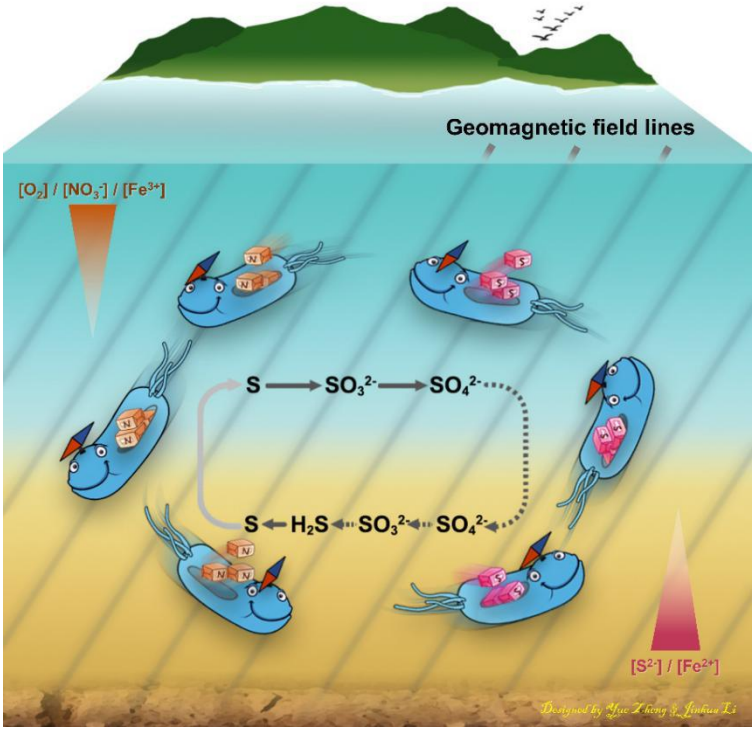

图 1. 这幅卡通图展示了趋磁细菌利用地磁场的定向作用，在水体中向上向下来回穿梭，不仅将不同类型化学物质上下运输，还将其在 OAI 上部的有氧代谢过程（硫氧化和硝酸盐吸收等）与 OAI 下部的厌氧代谢过程（硫酸盐还原、硫的部分还原及沉积和硝酸盐还原等）联动起来，从而促进细胞的生长和磁小体的生物矿化。

OAI 在自然界硫循环中作用巨大。通常而言，OAI 下部无氧环境中的硫化氢，需要被带到 OAI 上部的有氧环境下，才能被彻底氧化成硫酸盐。前人研究发现，微生物演化出多种策略，充当硫物质的“转运使者”或硫氧化-还原反应的电子“传递体”，并从中获得能量，供自己生长。比如，电缆细菌以头尾相接的方式组成一条上千个细胞长度的丝状结构，一头伸出沉积物连接氧气，一头扎入沉积物中吸收硫化物。在下部将硫化氢氧化成单质硫，同时释放电子，再通过身体上的纳米电缆把电子传递到上端，进行有氧呼吸，产生能量，以供细胞生长。与电缆细菌不同，纳米比亚嗜硫珠菌（迄今发现尺寸最大的单细胞细菌，可达 750 微米）在厌氧环境利用体内存储的硝酸盐将硫化氢氧化成单质硫（$S^{2-} \rightarrow S^0$），并以硫颗粒的形式暂时存贮起来（在光学显微镜下硫颗粒会发出闪烁夺目的光彩，使得整个纳米比亚嗜硫珠菌细胞泛着微微的“珠光”，像极了饱满圆润的珍珠，因而得名）。当受到水流或其他物理扰动，携带有大量硫颗粒的细胞被带到有氧环境后，会利用氧气将单质硫彻底氧化成硫酸盐（$S^0 \rightarrow SO_4^{2-}$），同时吸收并将大

量的硝酸盐存贮在囊泡中，以备无氧环境下氧化硫化氢所需。

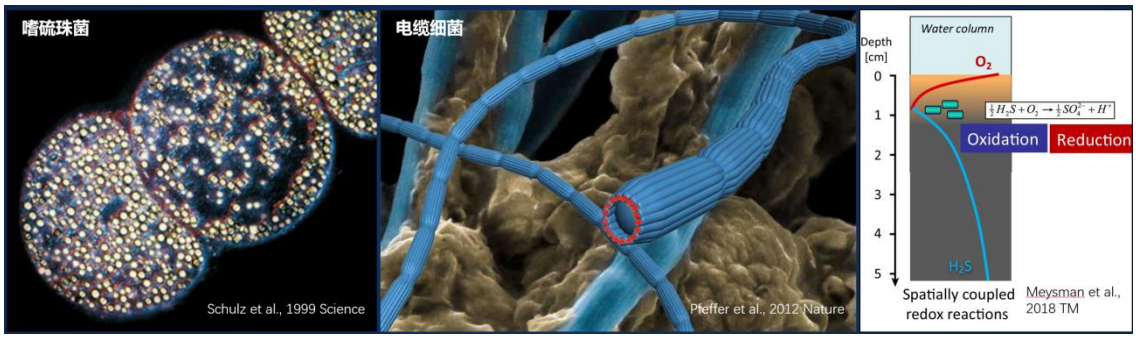

图 2. 各种硫细菌各显神通跨越“有氧-无氧界面”。电缆细菌充当硫氧化还原的电子传递体，而嗜硫珠菌充当硫物质的转运使者。

趋磁细菌是典型的梯度微生物，它们在全球水生环境中广泛分布，且集中生活在 OAI 界面或稍靠下的厌氧环境中。大量的观测发现，除了在细胞内矿化合成磁铁矿（Fe_3O_4）或胶黄铁矿（Fe_3S_4）颗粒外，很多趋磁细菌还可以在细胞内合成硫、多聚偏磷酸、脂质体、甚至碳酸钙等颗粒，指示趋磁细菌具有 C、N、P、S 和 Fe 等元素多样化的代谢潜能，及其在推动这些元素的地球化学循环中的潜在贡献。

1987 年，德国慕尼黑大学的古地磁学家 Nikolai Petersen 教授，在德国巴伐利亚州素有“巴伐利亚之海”称号的基姆湖中发现了一类独特的趋磁细菌，它细胞巨大，呈稍微弯曲的长杆状（有没有点酷似巴伐利亚大香肠的感觉哈），被命名为巴伐利亚趋磁大杆菌（Magnetobacterium bavaricum）。与通常只有 1-3 微米大小的单细胞趋磁细菌不同，巴伐利亚趋磁大杆菌直径约为 1.5 微米，长度可达约 8-10 微米，能在细胞内合成多达上千个子弹头形磁小体，还能合成大量的硫颗粒。这类有点像“趋磁细菌界航母”的大杆菌旋即引起趋磁细菌研究领域学者广泛地关注。然而，正如其形也独特，其性也高冷。迄今为止，大家只能在沉积物中观察到这类细菌，并不能在实验室通过纯培养技术获得该类细菌。2003-2004 年，受洪堡学者项目邀请，中国科学院地质与地球物理研究所潘永信研究员来到德国慕尼黑大学，他通过长达数月的仔细分离，从沉积物中获得富含巴伐利亚趋磁大杆菌的样品，并对这类细菌磁学性质及其对沉积物磁性的贡献进行了首次且系统的研究，相应成果发表在国际知名地学期刊 Earth and Planetary Science Letters 上（Pan et al., 2005a, b）。

2007 年，在巴伐利亚趋磁大杆菌被发现 20 年后的一天，潘永信研究员带领

博士生李金华和林巍等人，在北京的密云水库发现了密云水库趋磁大杆菌（命名为 Candidatus Magnetobacterium casensis strain MYR-1）。形态学和基因组学研究发现，密云水库趋磁大杆菌与巴伐利亚趋磁大杆菌高度相似，系统进化上归属于硝化螺旋菌门，属于同一个种的不同菌株（Lin et al., 2009, Lin et al., 2014）。为了系统研究密云水库趋磁大杆菌的磁学性质和生物矿化机制，课题组利用自行设计研制的趋磁细菌分离设备，从沉积物中富集和分离得到这类细菌后，综合岩石磁学和透射电子显微学技术，从细胞到原子水平研究了密云水库趋磁大杆菌子弹头型磁小体的宏观和微观磁性、磁小体链的组装模式、及其磁小体的晶体生长过程，发现了子弹头型磁小体的“多阶段晶体生长”规律，提出硝化螺菌门趋磁细菌子弹头型磁铁矿的生物矿化模型，并提出子弹头型磁铁矿的[001]拉长是更可靠化石磁小体判据的新观点（Li et al., 2010, 2015）。

图 3. 左图：慕尼黑大学 Nikolai Petersen 教授在德国基姆湖采集巴伐利亚趋磁大杆菌样品。右图：中科院地质地球物理研究所潘永信研究员带领博士生李金华在北京密云水库采集密云水库趋磁大杆菌样品。

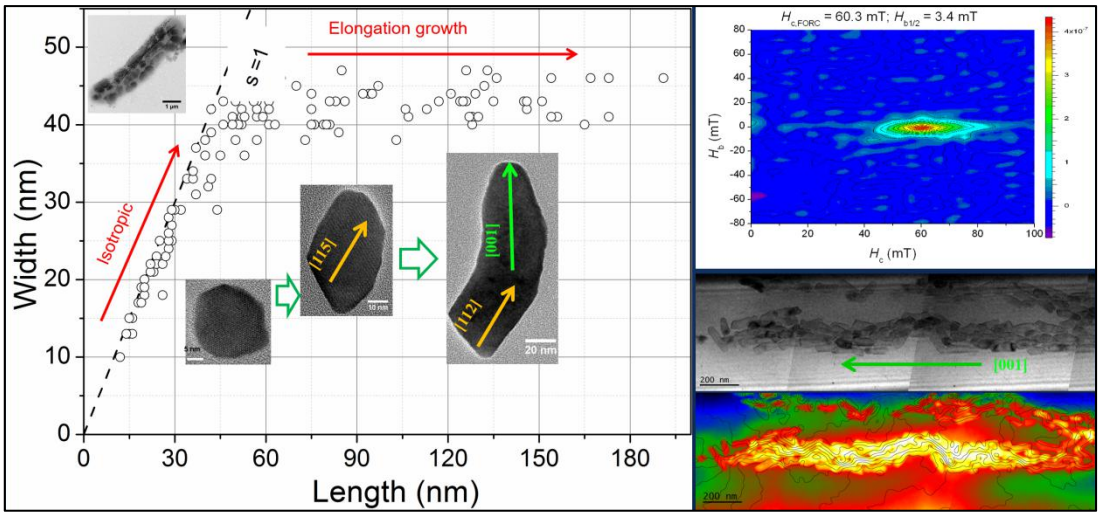

图 4. 密云水库趋磁大杆菌子弹头形磁小体的晶体生长机制、宏观和微观磁学性质（Li et al., 2015, 2020）。

2017 年，在密云水库趋磁大杆菌被发现 10 年后，李金华研究员与潘永信院士团队，又联合国内外合作者，建立了一种“荧光-电子显微镜联用”新技术（FISH-SEM 和 FISH-TEM），将趋磁细菌种类鉴定的荧光显微镜观测信号与磁小体结构观测的电子显微镜观测信号结合起来，为深入开展包括密云水库趋磁大杆菌在内的未培养趋磁细菌的研究开通了快车道（Li et al., 2017, 2019, 2020; Zhang et al., 2017; Liu et al., 2020）。同时，他们也在北京密云水库、天津于桥水库、河北东武仕水库和黑龙江大庆黑鱼湖等地也发现了与密云水库趋磁大杆菌同种的趋磁大杆菌。

为了继续认识趋磁大杆菌“趋磁性、生物矿化、生理代谢”三者之间的内在联系，研究团队联合加拿大同步辐射光源实验室和澳大利亚国立大学的合作者，综合透射电子显微学、同步辐射和单细胞宏基因组学技术对发现自天津于桥水库的趋磁大杆菌进行了深入研究。结果发现：1）除了已经发现的磁小体（M）、硫（S）和脂质体（L）颗粒外，趋磁大杆菌还能在细胞内形成第四种微米级别大小的囊泡（V）结构，扫描透射电镜电子能量色散谱（STEM-EDS）和同步辐射 X 射线吸收谱（STXM-XAS）分析表明，囊泡中不含有机物，可能是一种无机物的贮藏结构。统计分析显示，与所有细胞均含有磁小体不同，约 24.7%的细胞只含有硫颗粒，约 12.9%的细胞只含有囊泡，其余细胞（~ 62.4%）即不含硫颗粒，也不含囊泡。这指示硫与囊泡只是细胞内的“临时住户”，二者存在某种“此消彼长”的关系。2）同步辐射扫描透射 X 射线显微谱学（S L-吸收边的 X 射线近边结构谱，S L-边 STXM-XANES）分析表明，趋磁大杆菌细胞内的硫颗粒并不是通常认为的环状硫（S8）结构，而是线状结构，且朝向颗粒内部，其聚合度增加（e.g., $S^{3+} \rightarrow S^{5+}$），这可能指示这些硫颗粒处在从外到内的动态降解或合成过程中。3）C K-边的 STXM-XANES 分析表明，趋磁大杆菌细胞内的有机质及其分布具有显著的非均质性，多糖类物质主要分布在细胞外，为胞外多糖组织；脂类和芳香族类有机质在囊泡部位基本没有分布，而在其他部位特别是磁小体链部位显著存在，这与细胞质、磁小体膜及链有机质骨架相匹配；相比较，蛋白质在囊泡膜上显著分布，指示囊泡可能为富含蛋白酶的活性结构。4）N K-边 STXM-XANES 分析显示，囊泡与细胞其他部位的蛋白质种类及组成明显不同，且能检测到微弱的硝酸盐信号。同时，基因组分析显示趋磁大杆菌不含有合成气

泡的任何关键基因，但是具有合成液泡的关键基因，且存在一整套膜结合的硝酸盐还原酶基因。这些实验观察和基因证据均指示，趋磁大杆菌合成的囊泡是液泡，可能用来临时贮藏过多的硝酸盐。

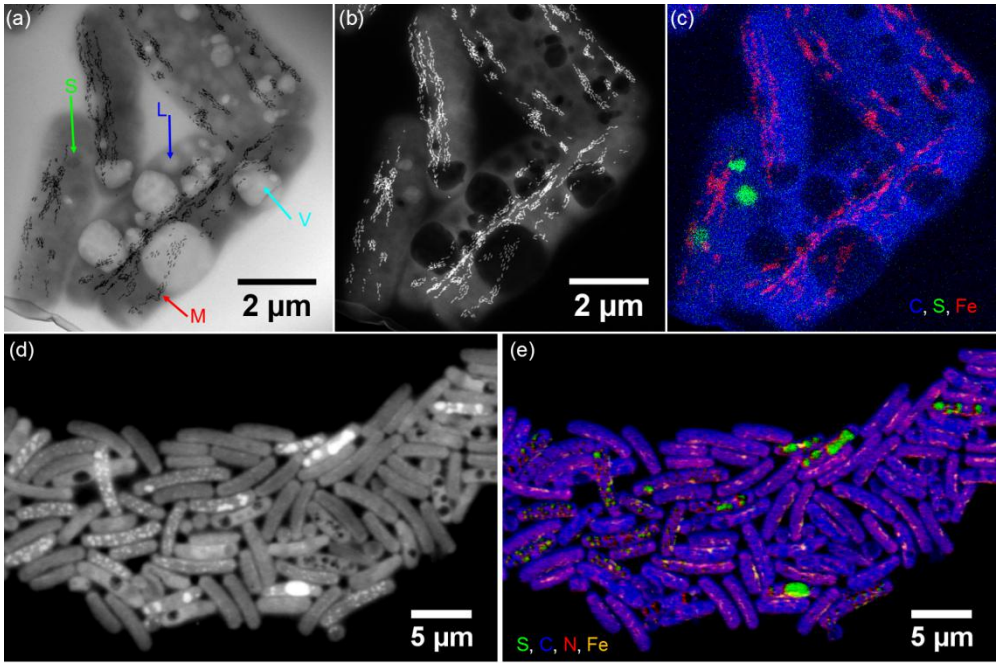

图 5. 扫描透射电镜电子能量色散谱（STEM-EDS）和同步辐射 X 射线吸收谱（STXM-XAS）研究趋磁大杆菌细胞结构和化学组成。

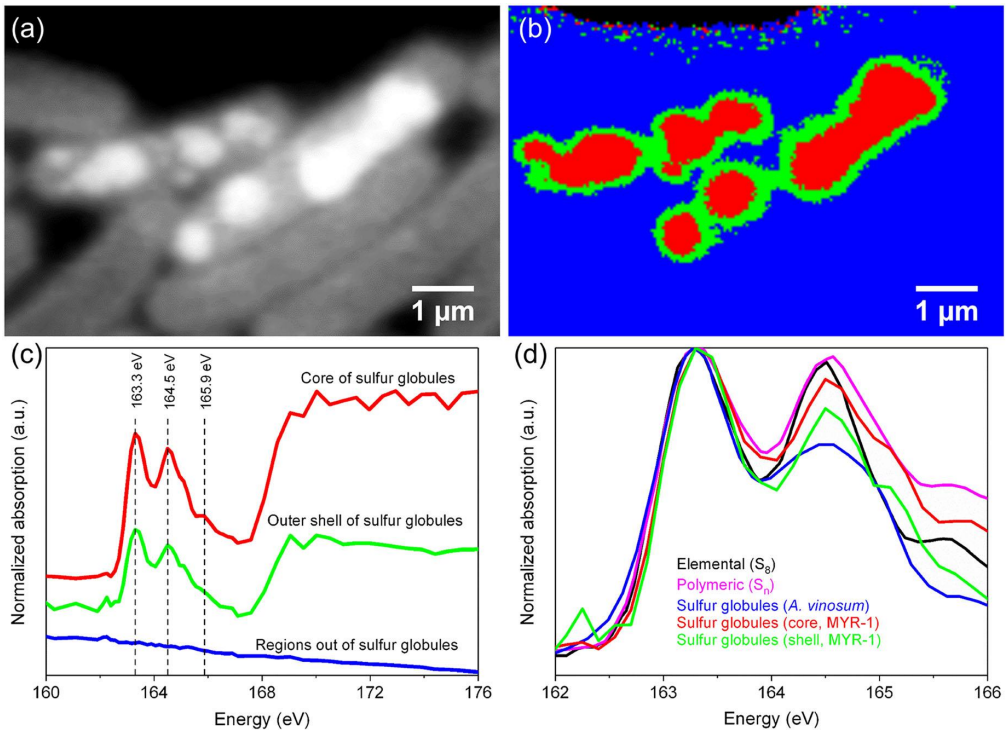

图 6. 同步辐射扫描透射 X-射线显微谱学技术(STXM-XANES)研究趋磁大杆菌细胞内硫颗粒的化学价态和结构。

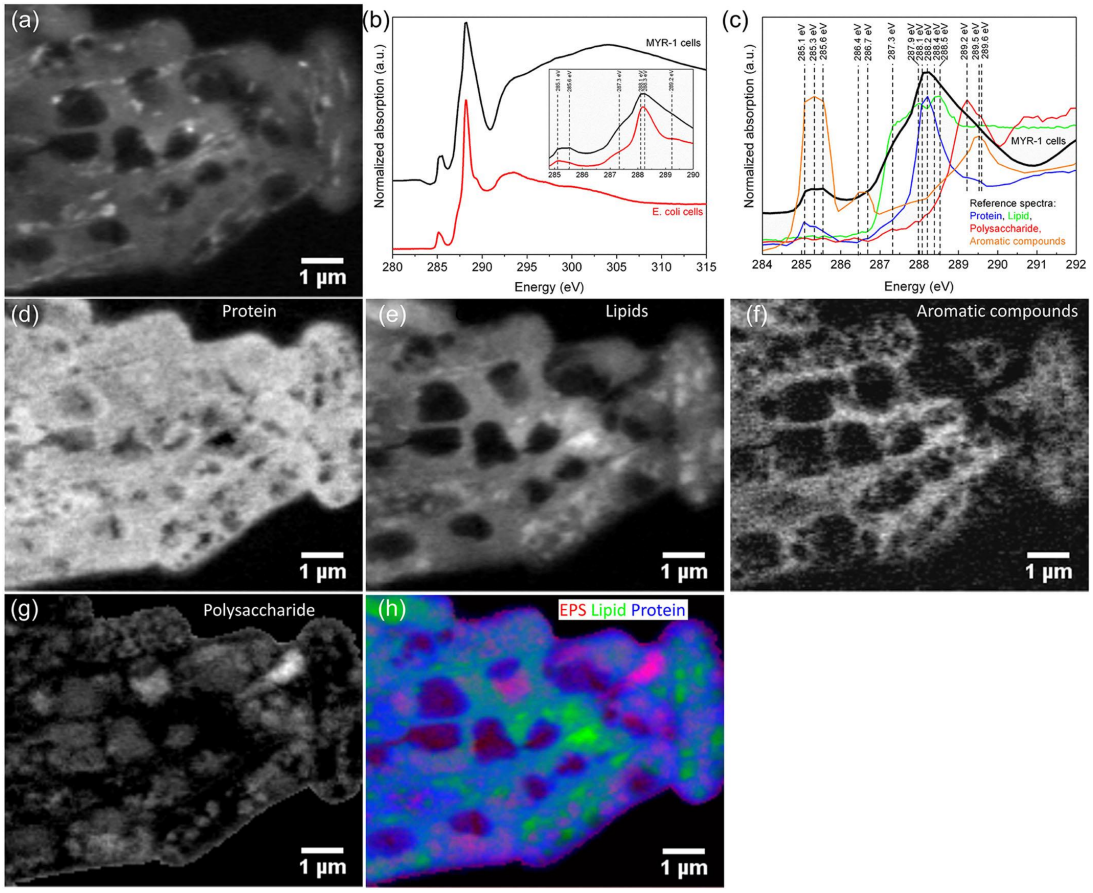

图 7. 同步辐射扫描透射 X-射线显微谱学技术(STXM-XANES)研究趋磁大杆菌细胞有机质种类及其分布特征。

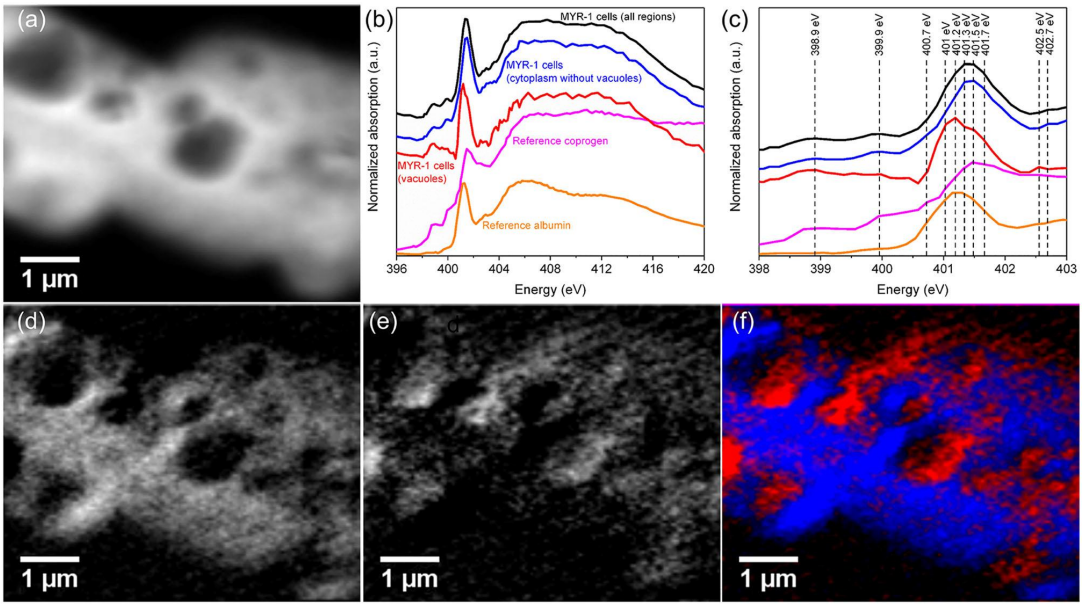

图 8. 同步辐射扫描透射 X-射线显微谱学技术(STXM-XANES)研究趋磁大杆菌细胞及囊泡部位蛋白质种类及分布。

综合我们与前人的研究结果，我们提出了趋磁大杆菌利用地磁场上下穿梭驱动硫循环的新模型。（1）在 OAI 下部的无氧环境中，趋磁大杆菌利用硝酸盐将硫化氢氧化成单质硫以颗粒的形式沉积在细胞内（$S^{2-}\rightarrow S^{0}$）；（2）为了继续完成硫的氧化，细菌需要向上游泳到 OAI 上部的有氧环境中；（3）在有氧环境中，细胞内存储的硫被彻底氧化成硫酸盐（$S^{0}\rightarrow SO_3^{2-}\rightarrow SO_4^{2-}$），同时吸收硝酸根并将其存储在液泡中；（4）怀揣硝酸盐的细菌再次向下游泳到 OAI 下部的无氧环境，为硫化氢的氧化提供氧化剂。由于北半球地磁场的磁力线是倾斜向下的，因此，在整个过程中，地磁场的定向作用可以把趋磁大杆菌的游动限定在一个近似“上下穿梭”的二维空间中，从而既提高了细菌的穿梭效率，又利于节省能量。另一方面，通过这种上下穿梭，趋磁大杆菌可以完成 Fe^{2+}和 Fe^{3+}的吸收及其氧化还原，从而合成大量混合价态的四氧化铁颗粒。数目众多的磁小体颗粒也为趋磁大杆菌克服局部扰动或沉积物颗粒阻挠，高效沿地磁场方向定向游泳提供保障。

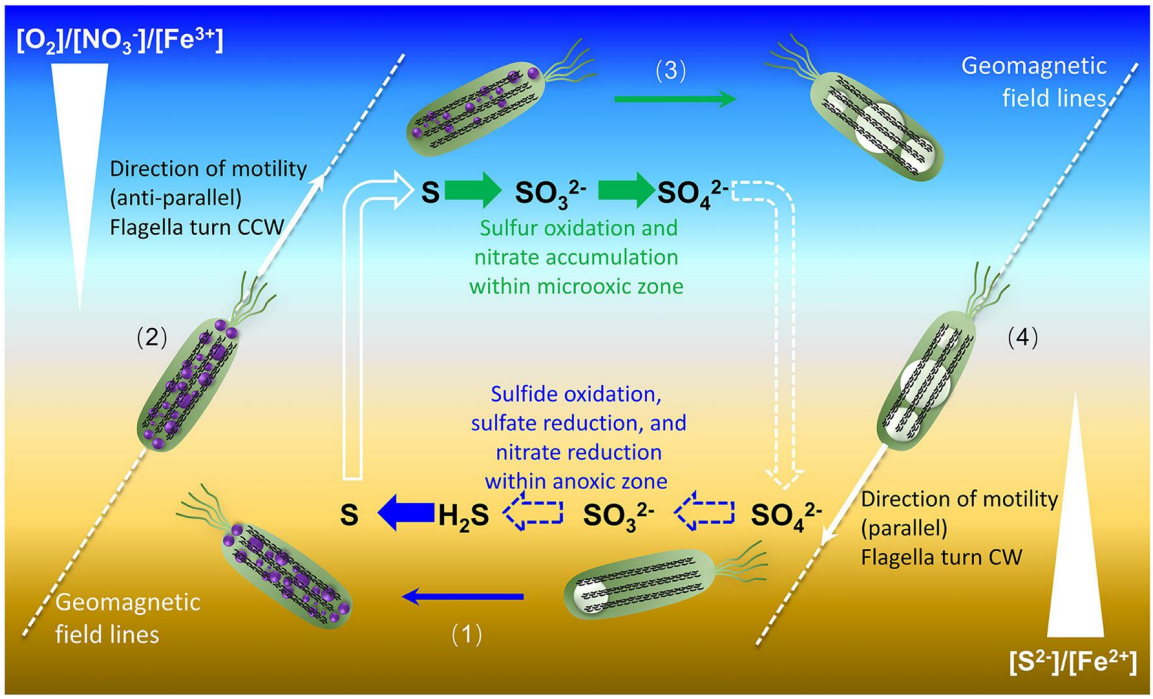

图 9. 趋磁大杆菌沿地磁场上下穿梭驱动硫循环模式图。

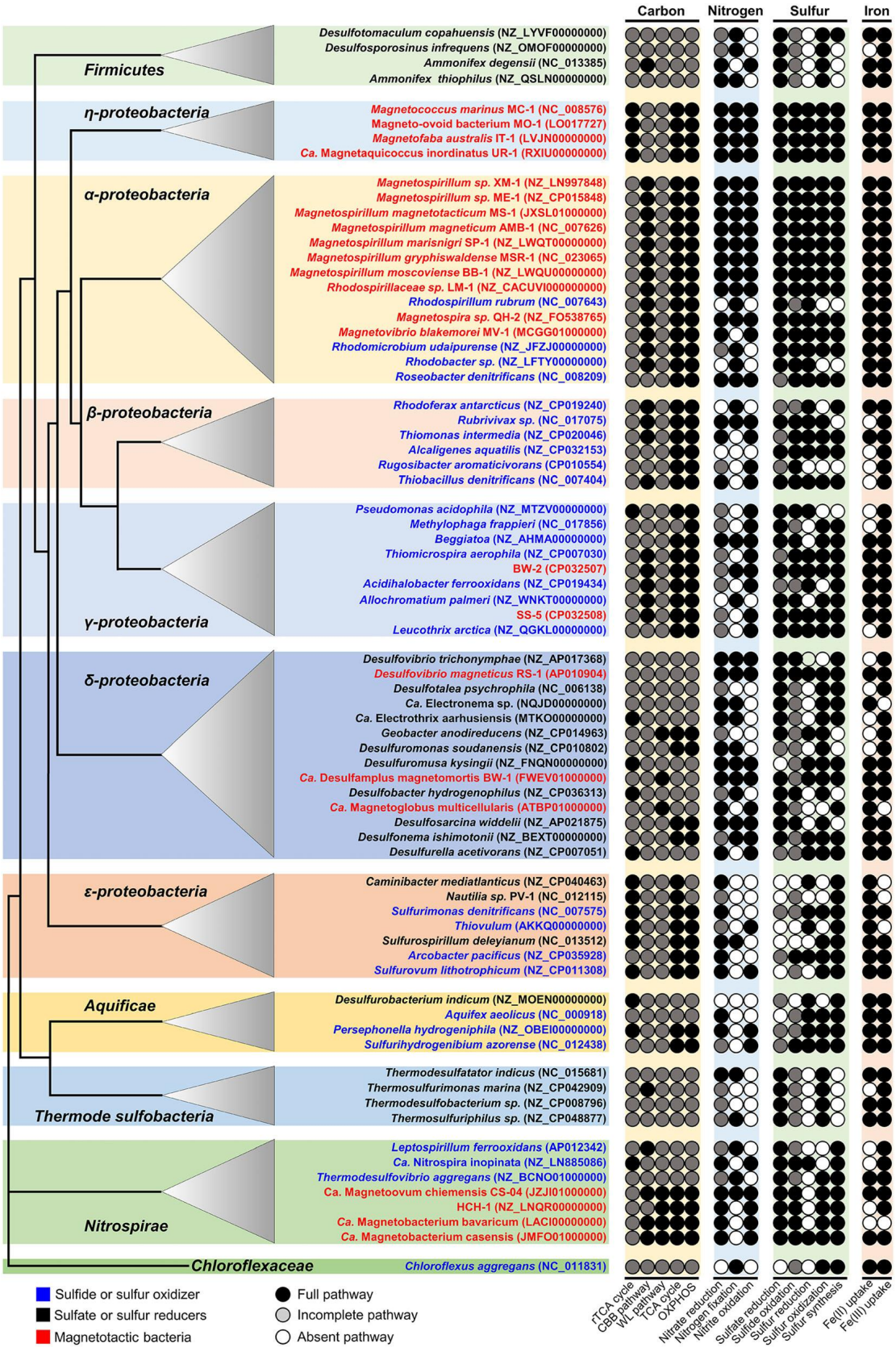

图 10. 基因预测分析揭示趋磁细菌具有碳、氮、硫和铁等元素多样化的代谢潜能，指示其是一类重要的微生物功能群，在地球水生环境的物质和能量循环中起重要作用。

其它趋磁细菌有没有可能采用同样的机制呢？我们通过基因组学对比分析了 84 种代表性趋磁细菌和硫细菌对碳、氮、硫和铁等元素的代谢潜能。基因预测分析表明，与其他硫细菌相比，趋磁细菌具有更加完善和全面的 Fe2+/Fe3+吸收途径，具有成套的磁小体矿化合成相关基因；具有完整的硝酸盐还原和亚硝酸盐氧化酶基因；具有完整的硫氧化（$S^{2-}\rightarrow S^{0}\rightarrow SO_3^{2-}\rightarrow SO_4^{2-}$）和硫酸盐还原（$SO_4^{2-}\rightarrow SO_3^{2-}\rightarrow S^{2-}$）关键酶基因。除了δ-变形菌纲趋磁细菌外，其他类群的趋磁细菌均具有碳固定的自养生长和有氧呼吸的异养生长相关的关键酶基因。这指示，趋磁细菌可能采用与趋磁大杆菌相似的策略，利用地磁场的定向作用，在水生环境的无氧环境和有氧环境中上下穿梭，从而驱动 OAI 中的碳、氮、硫、磷和铁等元素循环。这项研究揭示了趋磁细菌可以利用地磁场的定向作用，在水体有氧-无氧界面上下高效穿梭，从而驱动 OAI 环境中的物质和能量循环，既指示趋磁细菌是自然环境中驱动碳、氮、磷、硫、氧和铁等重要元素地球生物化学循环的重要微生物功能群，又表明趋磁细菌利用这种高效的穿梭机制，将“趋磁性、生物矿化、生理代谢”三者有机的联系起来，从而使自己能很好地适应厌氧和微氧环境，并从中获取细胞生长和磁小体合成所需要的能量和物质。

本项目研究受中国国家自然科学基金重点国际（地区）合作研究项(41920104009)、国家自然科学基金重大项目课题（41890843）和国家自然科学基金创新研究群体项目（41621004）资助。

该成果于 2020 年 11 月发表在《Journal of Geophysical Research: Solid Earth》上。Li J H, Liu P Y, Wang J, et al. Magnetotaxis as an adaptation to enable bacterial shuttling of microbial sulfur and sulfur cycling across aquatic oxic-anoxic interfaces. Journal of Geophysical Research: Biogeosciences, 2020, 125, e2020JG006012. https://doi.org/10.1029/2020JG006012

作者简介：李金华，中科院地质与地球物理研究所研究员，博士生导师。长期从事地球科学与生命科学的前沿交叉研究。获 2015 年度国家自然科学基金“优秀青年科学基金”资助和中国地球物理学会 2015 年“傅承义青年科技奖”称号。

张勇等，Journal of Geophysical Research: Solid Earth：大巴山褶皱冲断带的流体迁移及化学重磁化

由于挤压应力和重力的影响，造山作用会导致造山带流体从褶皱冲断带迁移到前陆盆地(Oliver，1986)。造山带流体在迁移过程中会导致多种地质现象的产生，例如沉积岩层的化学重磁化现象（Elmore et al., 2012），前陆盆地油气藏的形成和破坏（Zhang et al., 2018, 2019），低温沉积型矿床(如 MVT 铅锌矿)的形成（Lewchuk and Symons, 1995）等。这些在前陆盆地区域的地质过程和现象得到了较为广泛的研究，但造山带流体在褶皱冲断带区域是如何迁移以及相关地层是如何产生化学重磁化现象等问题还缺少相关的研究。

针对上述科学问题，南京大学地球科学与工程学院博士后张勇在该院贾东、李永祥教授及英国帝国理工学院 Adrian Muxworthy 教授的联合指导下，针对大巴山褶皱冲断带开展详细的造山带流体迁移和化学重磁化研究。大巴山褶皱冲断带是在晚三叠世古特提斯洋关闭后华北和华南块体持续碰撞产生的中晚侏罗世时期的造山带（Dong et al., 2013），包含冲断带和褶皱带两个构造单元，出露多种岩性地层，包括碳酸盐岩，泥岩，膏岩层，以及出露广泛的逆冲断层和不整面，是探索不同构造带，膏岩层，断层和不整面对造山带流体迁移影响的理想研究区域。通过详细地古地磁，岩石磁学，扫描电镜，Sr 同位素实验和分析，揭示了大巴山褶皱冲断带存在广泛的中晚侏罗世的化学重磁化现象。该文章论证了造山带流体的广泛交代作用及抬升和变形过程中氧化还原环境的变化是重磁化产生的机制，并揭示出造山带流体在冲断带和褶皱带的迁移模式存在差异，明显受控于逆冲断层，膏岩层，不整面等因素的影响。

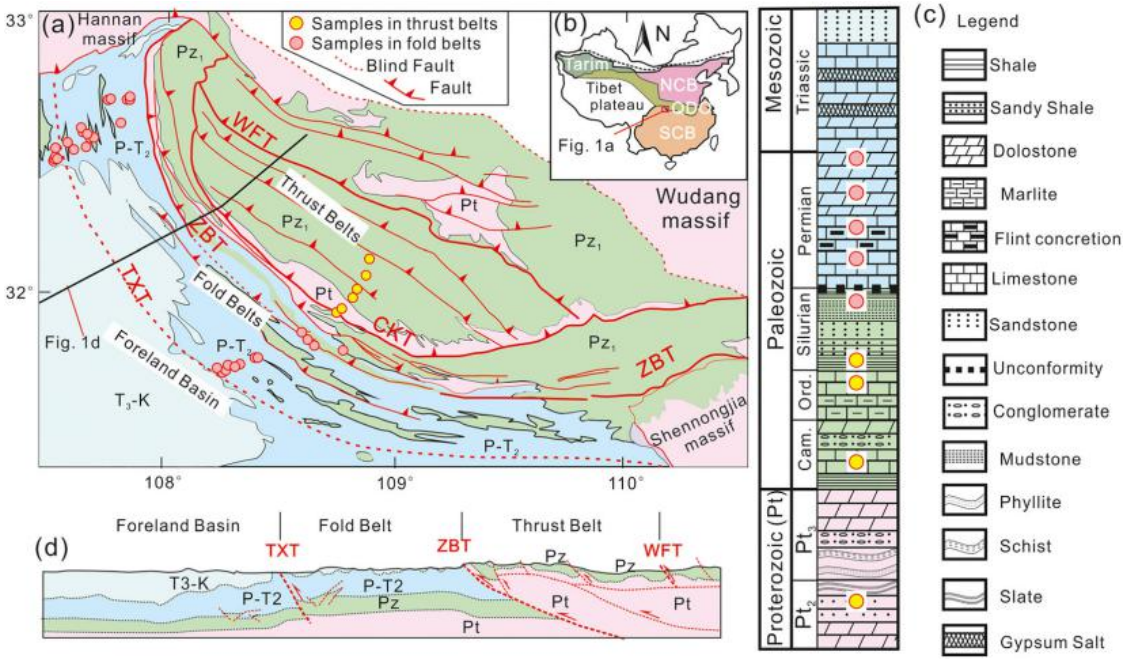

图 1

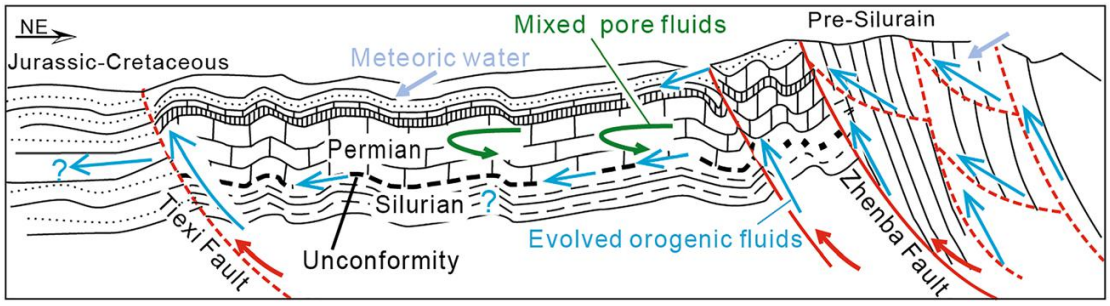

图 2

该成果于 2020 年 11 月发表在《Journal of Geophysical Research: Solid Earth》上。Zhang Y, Jia D, Muxworthy A R, et al. Fluid Migration and Widespread Remagnetization in the Dabashan Fold and Thrust Belt, China. Journal of Geophysical Research: Solid Earth, 2020, 125, e2020JB019989. https://doi.org/10.1029/2020JB019989

作者简介：第一作者为张勇博士，主要从事构造流体迁移，油气演化和成矿过程中的化学重磁化研究，2016 年博士毕业于南京大学，师从贾东和李永祥教授。现在南京大学地球科学与工程学院从事博士后的研究工作。

高亮等，Journal of Geophysical Research: Solid Earth：华南晚中生代与岩浆-热液过程有关的重磁化

古地磁研究通过分离岩石形成时所携带的原生特征剩磁为目标来进行古大陆重建，对板块构造理论提供了强有力的支撑。但随着古地磁的发展，在全世界不同地区发现了普遍的重磁化现象，也就是岩石的原生特征剩磁被岩石形成后的某些地质事件（热事件或者流体作用等）所重置，记录了这些地质事件发生时期的地球磁场信息。在这个过程中，次生的可携带稳定特征剩磁方向的磁性矿物，例如磁铁矿、赤铁矿和磁黄铁矿等的形成及剩磁获得所导致的重磁化被称为化学重磁化。在我国华南地区就存在着非常普遍的晚中生代化学重磁化现象，然而关于重磁化的机制仍然存在争议，这极大地限制了华南板块视极移曲线的建立，主要原因之一就是缺乏对次生磁性矿物形成过程的直接制约。

针对上述科学问题，中国地质大学（北京）高亮副教授在邓军、王庆飞、杨振宇和张世红教授指导下选取华南板块西缘晚泥盆世下雷锰矿为研究对象，进行了系统的野外地质调查、岩相学、构造古地磁学和岩石磁学研究，并创新性的结合了磁铁矿原位主微量元素分析，取得如下成果：

1. 通过系统的古地磁学与岩石磁学实验，从晚泥盆世下雷锰矿的矿石以及顶底板和夹层硅质岩中分离出了方向一致且稳定的高温特征剩磁分量，主要携磁矿物为磁铁矿，高温特征剩磁方向未通过褶皱检验，通过与华南板块视极移曲线对比，确定次生剩磁获得时间为晚中生代；

2. 通过系统的野外地质调查、岩相学以及原位主微量元素分析确定次生磁铁矿的形成与矽卡岩化过程有关，结合次生剩磁获得时间，证明岩浆-热液改造是华南地区晚中生代重磁化的重要机制；

3. 因此，综合以上研究结果以及前人的工作，提出下雷锰矿形成后，在晚中生代又受到岩浆-热液改造，发现古地磁学与矿床学相关研究方法的交叉对于同时解决重磁化和复合成矿的机制、过程及时间等科学问题具有一定优势。

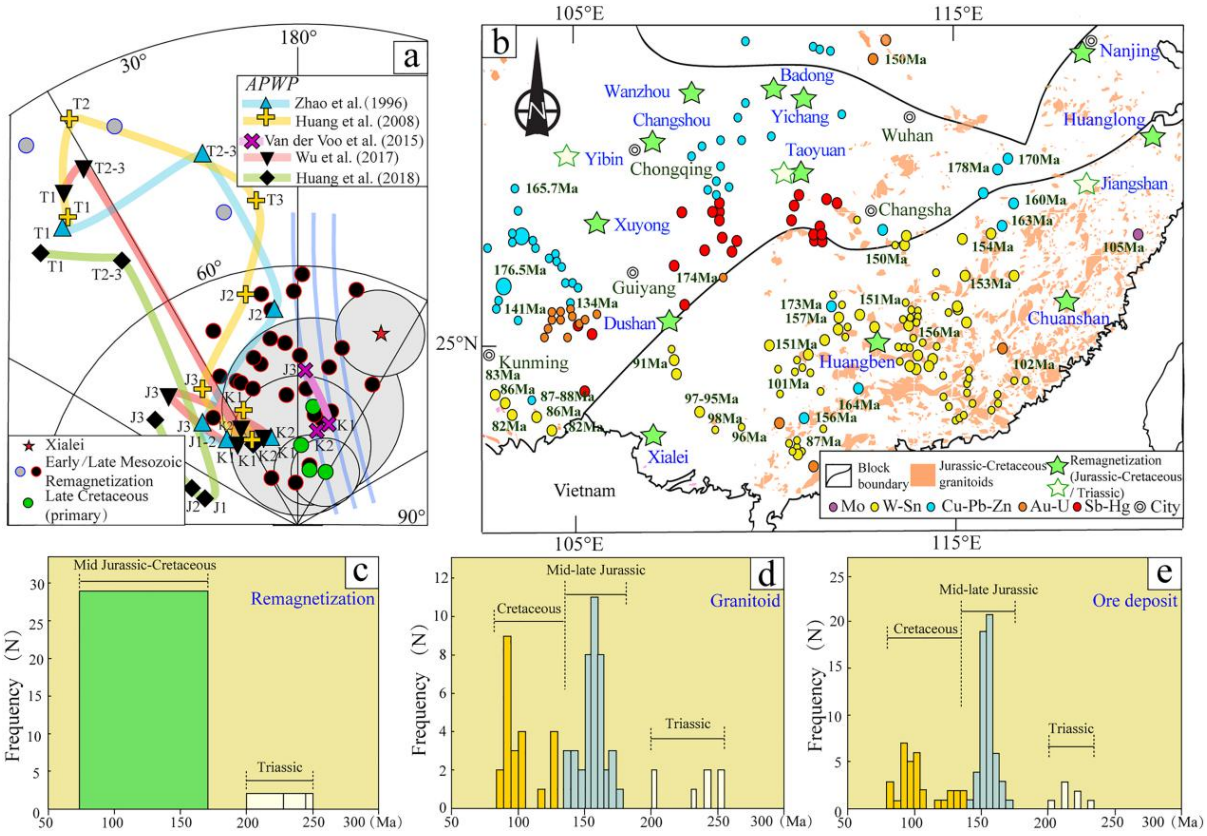

图 1 （a）使用视极移曲线限定下雷锰矿的重磁化时间为晚中生代；（b，c，d 和 e）重磁化事件与华南板块的岩浆-成矿事件的对比说明岩浆-热液改造是华南晚中生代重磁化的重要机制。

该成果发表在 《Journal of Geophysical Research: Solid Earth》 上：Gao L, Wang Q, Deng J, et al. Magmatic-Hydrothermal Alteration Mechanism for Late Mesozoic Remagnetization in the South China Block. Journal of Geophysical Research: Solid Earth, 2020, 124: 10704-10720.

作者简介：高亮，博士，中国地质大学（北京）海洋学院副教授，博士生导师，主要研究方向为南极地质与古地磁学。2016 年博士毕业于中国地质科学院地质力学研究所，之后进入中国地质大学（北京）博士后流动站，并留校工作。曾参加中国第 31、35、36 次南极科学考察、中-智联合南极科学考察和国际大洋发现计划（IODP）379 南极阿蒙森海航次。自 2016 年以来主持包括国家自然科学基金青年和面上项目、中国博士后科学基金面上项目和中国博士后国际交流计划等项目。在 Geology、JGR-Solid Earth 和 G-Cubed 等学术期刊发表论文 20 余篇。

磁学演译

第 42 章 大陆介质磁信息

1.1. 黄土和其他风成物质

风成黄土覆盖了全球 10%左右的陆地表面，主要位于中纬度地区（图 1）。形成黄土的粉尘（例如：来自塔克拉玛干沙漠塔里木盆地的粉尘）可以通过西风带输送到太平洋甚至更远（Sun et al., 2008）。亚洲被认为是格陵兰冰芯中粉尘的源区（e.g., Biscaye et al., 1997）。因此，虽然黄土起源于其周围的沙漠，但是无法直接确定其来源。

中国中部的黄土（厚度 100-300 m）覆盖面积非常广（~ 500 × 10^6 km^2），是二百五十万年来良好的古气候载体（Heller and Liu, 1986; Kukla et al., 1988; Maher and Thompson, 1991, 1992, 1995; Banerjee and Hunt, 1993; An and Porter, 1997; Ding et al., 2002）及古气候研究对象（Heller and Liu, 1982, 1984; Heller and Evans, 1995; Guo et al., 1999; Zhu et al., 1999; Evans and Heller, 2001; Pan et al., 2001）。中国黄土高原黄土序列可能的来源包括戈壁沙漠以及西北部的三个盆地（准葛尔、塔里木、柴达木盆地）。根据电子自旋共振（ESR）信号强度和细粒石英的结晶度，Sun et al.（2008）认为黄土高原细粒黄土主要来源于北部，包括中国北部的戈壁和沙漠。在北美和欧洲，大部分黄土来源于冰川地区的岩石粉末。因此与中国黄土相比厚度较浅（一般< ~ 30 m）。虽然不同地区物源相差很大，但是有一个相同的特征即母质的磁性矿物含量较低。在新西兰（Pillans and Wright, 1990）、阿拉斯加（Begét et al., 1990; Lagroix and Banerjee, 2004; Lagroix et al., 2004）和阿根廷（Carter-Stiglitz et al., 2006; Bidegain et al., 2009）黄土中包含有磁学性质大不相同的火山灰，因而增加了解释黄土/古土壤磁学信号的复杂性。Liu et al.（2010）发现阿根廷土壤中母岩的磁化率贡献了 60%的磁性信号，除非不同粒度磁性矿物对磁学性质的贡献能够区分清楚，否则母岩与成土作用的磁学性质很容易混淆。环境磁学通过对经受风蚀的疏松沉积物表面的研究，探讨了气候变化对风成粉尘中磁性矿物的影响（Walden et al., 2000; Lyons et al., 2010），确定了风成沉积物（主要为黄土）的源区（Torii et al., 2001; Maher et al., 2009a, b）。

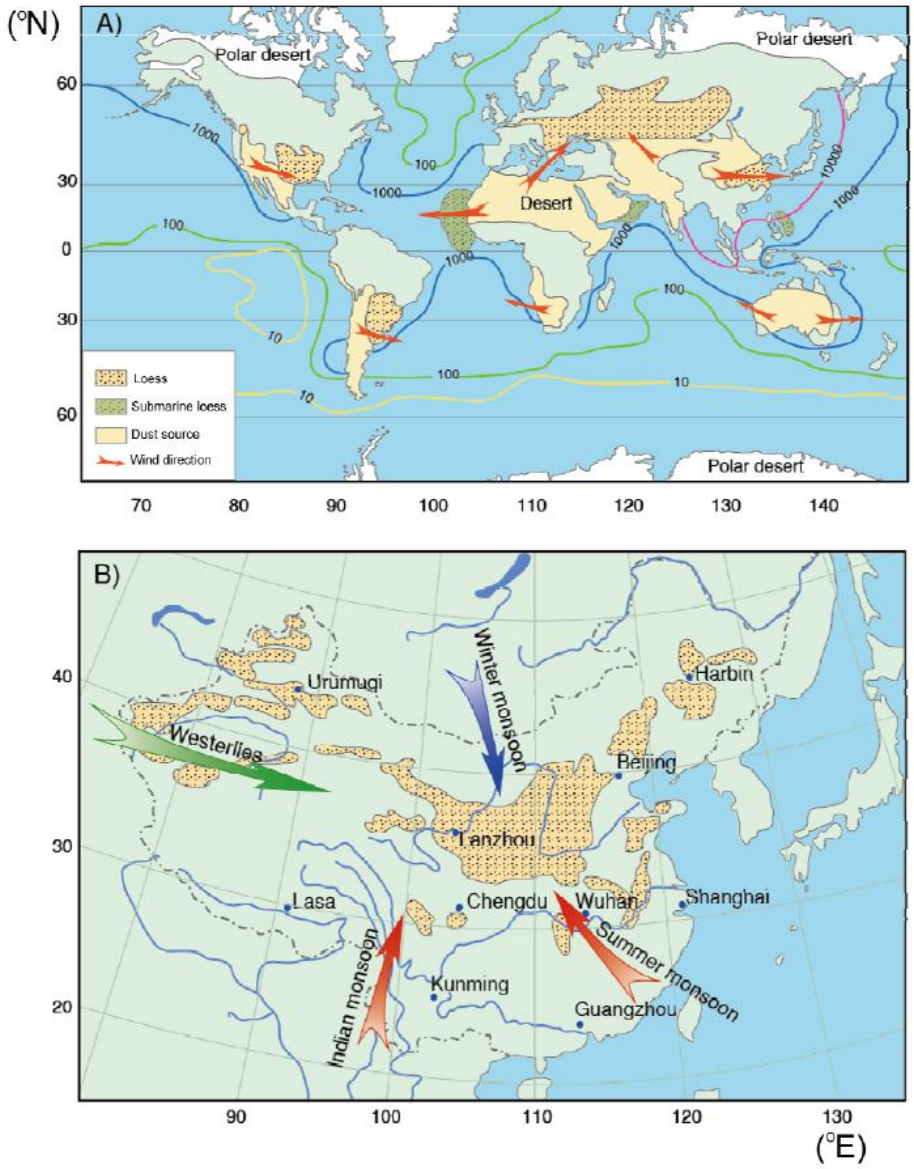

图 1. (A) 全球粉尘源区和沉积区分布图，粉尘通量等高线（mg m^{-2} yr^{-1}）分布在源区周围的海洋中（修改自 Duce et al.（1991））; (B) 中国的黄土沉积分布，箭头指示风向。

1.2. 冲积河流沉积物

冲积河流沉积物可以长时间（达百万年）连续沉积（达几千米）。这些沉积物常富含铁氧化物，其含量和粒径的变化可以反映气候的长期变化，但是却很难实现，因为这些环境下普遍缺乏高精度的古环境（如古生物）数据。尽管如此，大多数冲积河流沉积物还是成为环境磁学研究的焦点，这主要是因为它们是陆源沉积物的主要来源，也经历了成土作用（见 1.3 节）（White and Walden, 1997; Pope and Millington, 2000; Bógalo et al., 2001; Kumaravel et al., 2005;

Sinha et al., 2007; Franke et al., 2009; Gómez-Paccard et al., 2012）。除了其环境意义，河流沉积物源到汇的研究有助于解释海洋沉积记录（比如, Salomé and Meynadier, 2004; Horng and Roberts, 2006; Horng and Huh, 2011）。 例如，确定大陆架海洋沉积物中的磁性矿物是否含碎屑或成岩来源是很关键的。通过河流系统追踪磁性矿物是一种确定其来源的有效方式，尤其是在大量物源涌入的位置，通常与台风或风暴事件从物源搬运至沉积区有关（Salomé and Meynadier, 2004; Horng and Roberts, 2006; Horng and Huh, 2011）。

1.3. 湖泊沉积物

湖泊沉积物很重要，因为他们保存了高精度连续的大陆古气候信息。最早应用磁学方法研究湖泊沉积物可追溯到 1920 年（Ising, 1943）。Ising（1943）在湖泊纹泥开创性的研究中发现玛珥湖春季的沉积物中磁铁矿的含量比其它季节的高，这指示了湖泊沉积物的磁学性质受环境因素控制，尽管当时并不能完全解释其中的机制。1960-1980 年期间，英国湖泊磁学小组推动了湖泊沉积物环境磁学研究的突破性发展（Thompson, 1973; Thompson et al., 1975, 1980; Dearing and Flower, 1982; Sandgren and Snowball, 2002）。从此，利用磁学方法研究湖泊沉积物在国际上得到广泛应用。

湖泊沉积物中铁氧化物的变化（成分、含量、粒径）通过各种过程与气候密切相关，如湖区土壤发育、侵蚀类型（如水、冰）、集水区的侵蚀及湖泊内的有机碳产量及沉积后过程。土壤发育和侵蚀类型影响磁性矿物组合中的陆源组分，而生物生产力控制有机碳含量，其影响陆源铁氧化物的溶解及生物与自生成因的次生磁性矿物的生成（比如生物成因磁铁矿和胶黄铁矿）。非稳定态成岩过程，包括氧化与缺氧状态间的转换，可以由古环境指示并根据沉积物性质轻易检测出来（Williamson et al., 1999）。图 2 概括了湖泊－源区系统中磁性矿物的运移、沉积及沉积后改造的详细过程。

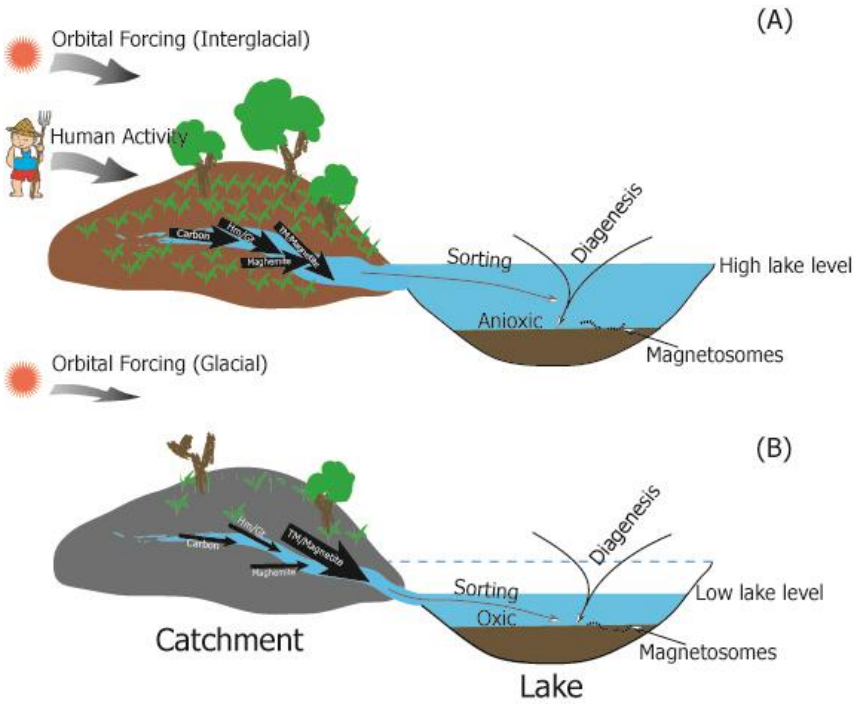

图 2. 湖泊集水系统中磁性矿物搬运、沉积和沉积后改造作用的概念模型。

（A）间冰期，（B）冰期。首先，全球气候背景（轨道应力）影响局部的气候和环境。在全新世，人类活动也影响了局部环境。集水区植被的扩张指示了全新世温和的气候条件，这会增加碳、赤铁矿/针铁矿以及溶解的营养物质输入，但是会使剥蚀和岩性输入减少。这种情况会促进成岩作用过程，加速湖内磁性矿物溶解。冷期时属于相反过程，图中箭头的粗细代表了释放到湖中的物质的含量变化。

前人研究表明格陵兰-北大西洋与大陆环境-气候变化强烈遥相关。通过研究贝加尔湖的生物硅记录，Colman et al.（1995）发现大陆内部的气候与全球气候系统相互作用，主要通过海洋-冰盖对轨道驱动（10 万年周期）的非线性响应，还有部分受太阳直接辐射影响。千年尺度上，Thouveny et al.（1994）发现法国中部地块的玛珥湖沉积物的磁化率与格陵兰冰芯 GRIP 和 GISP2 气候记录惊人的一致。利用冰期前沉积物的磁学性质可以合理解释与北大西洋气候变化相关的高山冰川活动问题（Lie et al., 2004; Nesje et al., 2006; Larrasoaña et al., 2010）。毋庸置疑，尽管湖泊区域的气候-环境变化首先受到全球气候背景控制，但对于最近的沉积物，人类活动（例如：采掘业、清理土地、火灾、过度放牧、富营养化、集水区过度建设等）也会对区域环境产生重要影响（Dearing et al., 1981; Higgitt et al., 1991; van der Post et al., 1997; Lanci et al., 1999; Gedye

et al., 2000; Hirt et al., 2003; Oldfield et al., 2003）。当沉积后的影响有限时，磁性矿物的含量可以用来半定量指示湖区的沉积通量（Dearing et al., 1981; Dearing and Flower, 1982）。但是，磁性矿物的总体磁性是变化多端并相互作用的各种过程（包括气候因素）的综合反映。比如，冰缘气候转变为温和的气候适宜湖区的植被生长，从而使碳通量和溶解氮增加，但冻融活动减弱导致侵蚀减少，表面凝聚力增强，陆源输入减少。因此，准确厘定湖泊沉积物中磁性矿物的来源对于解译环境信息是相当必要的。通常，风化产生的磁性矿物粒度较粗（PSD/MD）。但是，湖区中原生磁性矿物（如钛磁铁矿、磁铁矿）的转变会带来复杂性。成土作用产生 SP/SD 的磁赤铁矿和赤铁矿，因此湖泊沉积物中磁性矿物粒径的变化、磁赤铁矿与赤铁矿的相对含量可以用来追溯源区可能的风化过程。比如，在 Klamath 湖（美国俄勒冈州），S 比值的减少对应风化程度增强（Rosenbaum and Reynolds, 2004）。并且，陆源碎屑在沉积到湖底之前，在运移过程中可能因为水动力的分选使粗颗粒逐渐减少从而改变其中的磁性矿物（Rosenbaum and Reynolds, 2004）。

磁性矿物的性质与很多过程密切相关，比如源区的侵蚀历史、土地利用变化。 通常重要的是表面侵蚀与沟壑侵蚀间的平衡，雨水冲刷与小河发育引起表面侵蚀，主要作用于风化层，而沟壑侵蚀冲走更多未风化的土壤（Oldfield et al., 1979; Walling et al., 1979）。因此，为了精确解释湖泊沉积物中磁性矿物所韵含的古环境信息，我们需要了解湖泊沉积物与源区物质间的联系。湖泊-源区系统主要有 3 部分组成：源区物源（基岩、土壤等）、运移路径中的物质(漫滩沉积物、河床沉积物、河流悬浮物)和湖泊沉积物。实例中通常同时研究湖泊沉积物和源区物质。Oldfield et al.（1979）研究表明磁性参数在区别源区的不同磁性矿物方面很敏感。Dearing et al.（2001）对湖泊沉积物与源区物质的关系进行了十分系统的研究，他们研究了法国 Petit Lac d’Annecy 中部平原的湖泊沉积物，两个漫滩钻孔，河床沉积物和源区的几百个土壤样品。湖泊沉积物中还经常有磁性矿物浓度的孤立峰值。这样的峰值往往涉及到火山灰层，微滑塌层（高密度搬运和沉积的沉积物）（Ryves et al., 1996）或氧化还原环境快速变化导致胶黄铁矿的形成（Snowball and Thompson, 1990; Snowball, 1991; Roberts et al., 1996），当然其他机制也有可能。总体而言，虽然个别事件（如

洪水，滑塌，火山爆发等）和成岩作用对湖泊沉积物的磁性记录有很大的影响，这些材料仍然是陆地环境变化的一个重要信息来源。

1.4. 其它陆相材料

除了沉积物和土壤，其他材料也可以提供大陆古气候变化的环境磁学记录。这些材料包括极地冰盖、高山冰川和石笋。格陵兰冰芯（NGRIP）的环境记录研究表明粉尘含量和磁性矿物的浓度密切相关，这是由冰期-间冰期气候变化调控的（Lanci et al., 2004; Lanci and Kent, 2006; Lanci et al., 2012）。在 NGRIP 冰芯样品中的磁性矿物包括磁铁矿/磁赤铁矿和赤铁矿的混合物，且不随时间改变，这与中国黄土相似（cf. Biscaye et al., 1997），都为东亚起源（Lanci et al., 2004; Lanci and Kent, 2006）。 南极冰芯的磁学性质表明磁性颗粒浓度和气候变化之间没有明确的联系，相反，矫顽力的变化指示矿物类型及其来源在冰期-间冰期时间尺度有明显差异（Lanci et al., 2008, 2012）。位于塔克拉玛干沙漠和中国黄土高原之间的冰盖的初步岩石磁学研究还表明粉尘通量和来源在冰期-间冰期时间尺度存在差异，这进一步说明冰芯的岩石磁学性质具有记录冰芯中粉尘浓度、粒径及来源变化的潜在能力（Maher, 2011）。

前人研究表明，常规的岩石磁学技术可以对石笋中磁性矿物的浓度进行测量（Perkins, 1996; Openshaw et al., 1997; Lascu and Feinberg, 2011）。虽然对于石笋的岩石磁学研究的主要兴趣一直局限于地磁场记录的可靠性（主要为长期变和地磁倒转）问题，但碎屑的天然磁化强度屡见不鲜表明，根据准确的 U-Th 年龄，石笋的环境磁学研究可能提供有用的气候变化记录（e.g., Perkins, 1996; Lascu and Feinberg, 2011）。

文献速递

1. 大西洋多金属结壳地球化学记录的米兰科维奇旋回证据

翻译人：仲义 zhongy@sustech.edu.cn

Josso P, van Peer T, Horstwood M S A, et al. ***Geochemical evidence of Milankovitch cycles in Atlantic Ocean ferromanganese crusts*** *[J]. Earth and Planetary Science Letters, 2020, On line. https://doi.org/10.1016/j.epsl.2020.116651*

摘要：水成型多金属结壳被认为是大陆壳体风化作用影响下海水同位素组成的可靠记录。由于他们在地球上 400-7000 米深处的所有海洋中无处不在，它们形成了关于水团混合和气候分布最均匀且容易获得的记录之一。然后，由于其较低沉积速率和较差的年代限制使得我们无法寻找 100ka 周期的古气候信息。因此，在古新世气候岁差的控制下，东北大西洋的多金属结壳中铅同位素特征和主要元素含量可以很好记录西非降雨的强度和及其影响范围变化。利用高空间分辨率（4μm）激光剥蚀电感耦合等离子体质谱仪（LA-MC-ICP-MS）Pb 同位素数据在时空分辨率上比微钻取样精度上提高了 2 个数量级。记录结果证实，在单个铁锰氧化物层 $^{206}Pb/^{204}Pb$，$^{208,}{}^{207}Pb/^{206}Pb$ 比值，与 Fe/Mn 比值变化、Al、Si 和 Ti 的变化一致。对 Pb 同位素时间域和轨道调谐的结果证实了~20 ka、100 和 405 ka 周期的存在，其 1.5-3.5 mm/Ma 的生长速率与化学地层年代模型较为一致。在这一背景下，近日点北方夏季在西非造成了更强的日照，导致季风性降水比远日点的北方夏季更加强烈且地理范围更广。反过来，又会影响东北大西洋盆地的风化端元之间的平衡。这些结果为铁锰结壳记录校准提供了一种方法，并使我们的同位素和化学元素结果来探索 1000-5000 年来时间分辨率。

ABSTRACT: Hydrogenetic ferromanganese crusts are considered a faithful record of the isotopic composition of seawater influenced by weathering processes of continental masses. Given their ubiquitous presence in all oceans of the planet at depths of 400–7000 meters, they form one of the most well-distributed and accessible records of water-mass mixing and climate. However, their slow accumulation rate and poor age constraints have to date limited their use to explore 100 ka

paleoclimatic phenomena. Here it is shown how the Pb isotope signature and major element content of a Fe-Mn crust from the north-east Atlantic responded to changes in the intensity and geographic extent of monsoonal rainfall over West Africa, as controlled by climatic precession during the Paleocene. The studied high-spatial resolution (4 μm) laserablation multi-collector inductively coupled plasma mass spectrometer (LA-MC-ICP-MS) Pb isotope data is a nearly 2 order of magnitude improvement in spatial and temporal resolution compared to micro-drill subsamples. The record demonstrates cyclicity of the $^{206}Pb/^{204}Pb$ and $^{208,\ 207}Pb/^{206}Pb$ ratios at the scale of single Fe-Mn oxide laminae, in conjunction with variations in the Fe/Mn ratio, Al, Si and Ti content. Time-frequency analysis and astronomical tuning of the Pb isotope data demonstrates the imprint of climatic precession (~ 20 ka) modulated by eccentricity (~ 100 and 405 ka), yielding growth rates of 1.5–3.5 mm/Ma consistent with previous chemostratigraphic age models. In this context, boreal summer at the perihelion causes stronger insolation over West Africa, resulting in more intense and geographically extended monsoonal rainfalls compared to aphelion boreal summer conditions. This, in turn, influences the balance between the weathering endmembers feeding the north-east Atlantic basin. These results provide a new approach for calibrating Fe-Mn crust records to astronomical solutions, and allow their isotopic and chemical archive to be exploited with an improved temporal resolution of 1000–5000 years.

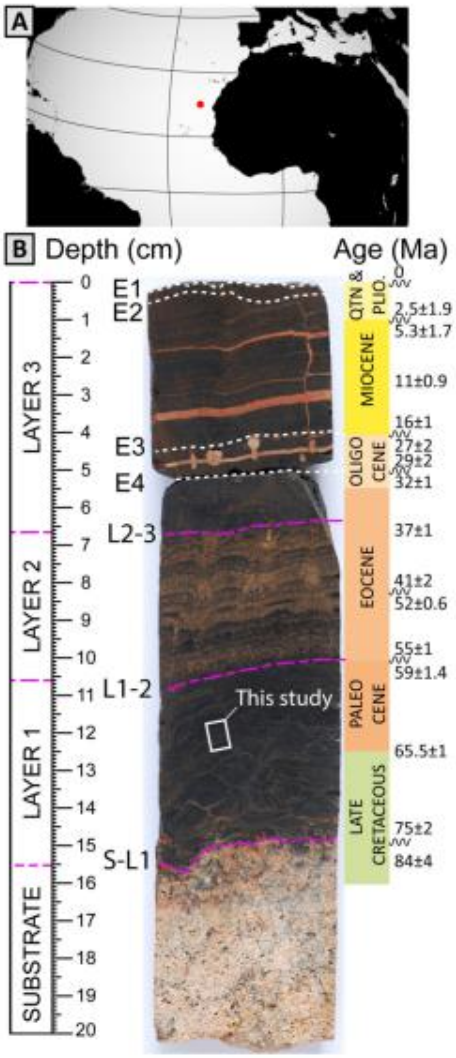

Figure 1. (A) Location of Tropic Seamount in the north-east Atlantic. (B) Cut section of core 085_004 showing the presence of three Fe-Mn oxide macro-layers resting on a carbonate substrate (modified from Josso et al. (2020b)). The white rectangle highlights the zone of interest for this study. An electron-back-scatter map of this area is presented in Fig. 2. See Josso et al. (2019) for details on establishment of the age model and Josso et al. (2020b) for a complete description of the geochemistry and textures of the core. (For interpretation of the colours in the figure(s), the reader is referred to the web version of this article.)

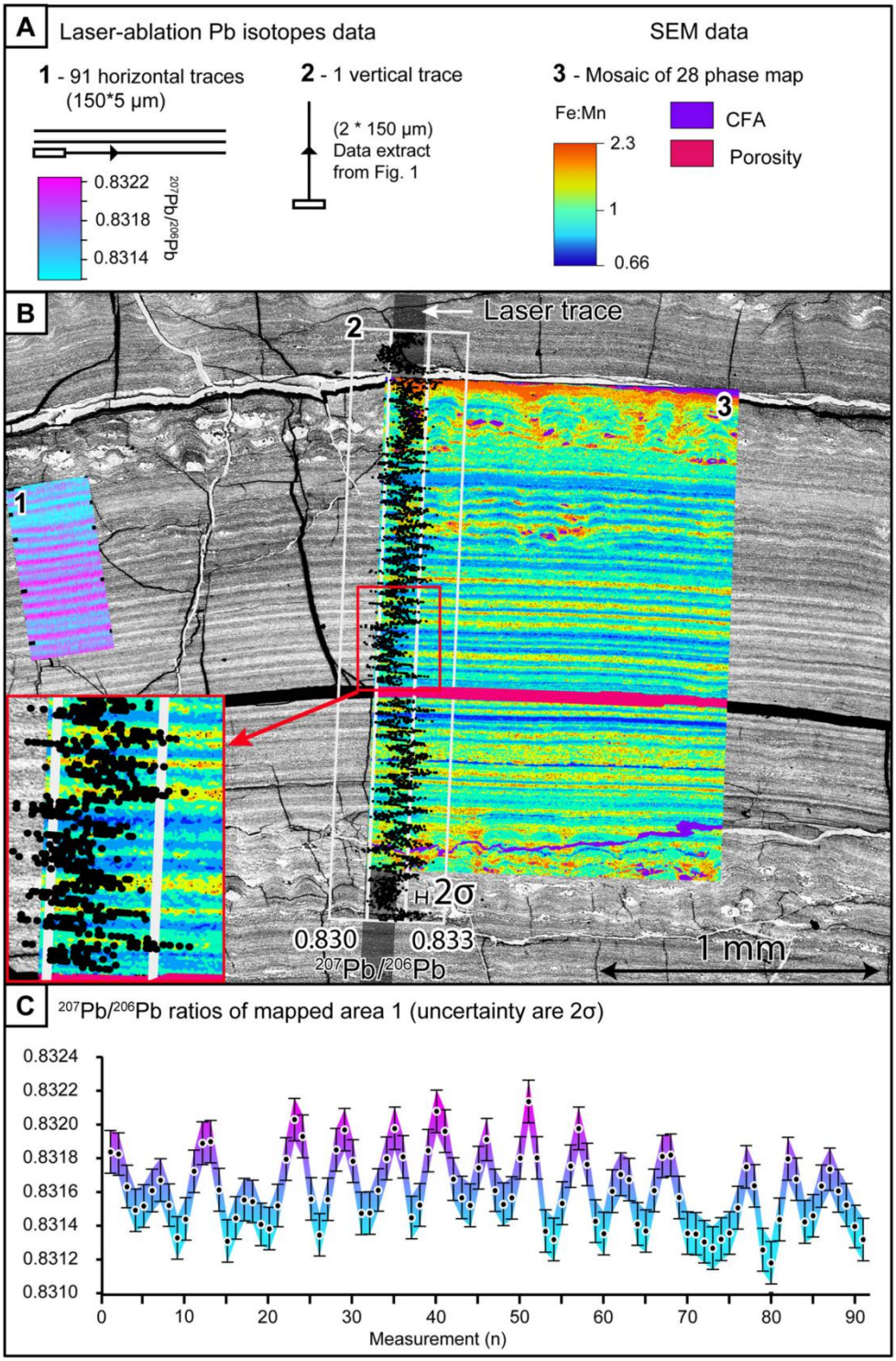

Figure 2. (A) Details of the laser-ablation pattern that produced the Pb isotope map 1, the Pb isotope dataset used for cyclostratigraphic analysis (2) and keys to colour scale of the Pb isotope map and SEM phase mapping (map 3) in panel B. CFA = carbonate-fluoro-apatite. (B) Geochemical phase mapping and 207Pb/206Pb mapping and transect data as shown on Fig. 2. This data and the close up demonstrate the positive correlation between high Fe/Mn ratio and high $^{207}Pb/^{206}Pb$ ratio. (C) Details of

the Pb isotope data produced during the 91 ablation traces used to produce map 1 using similar colour-coding.

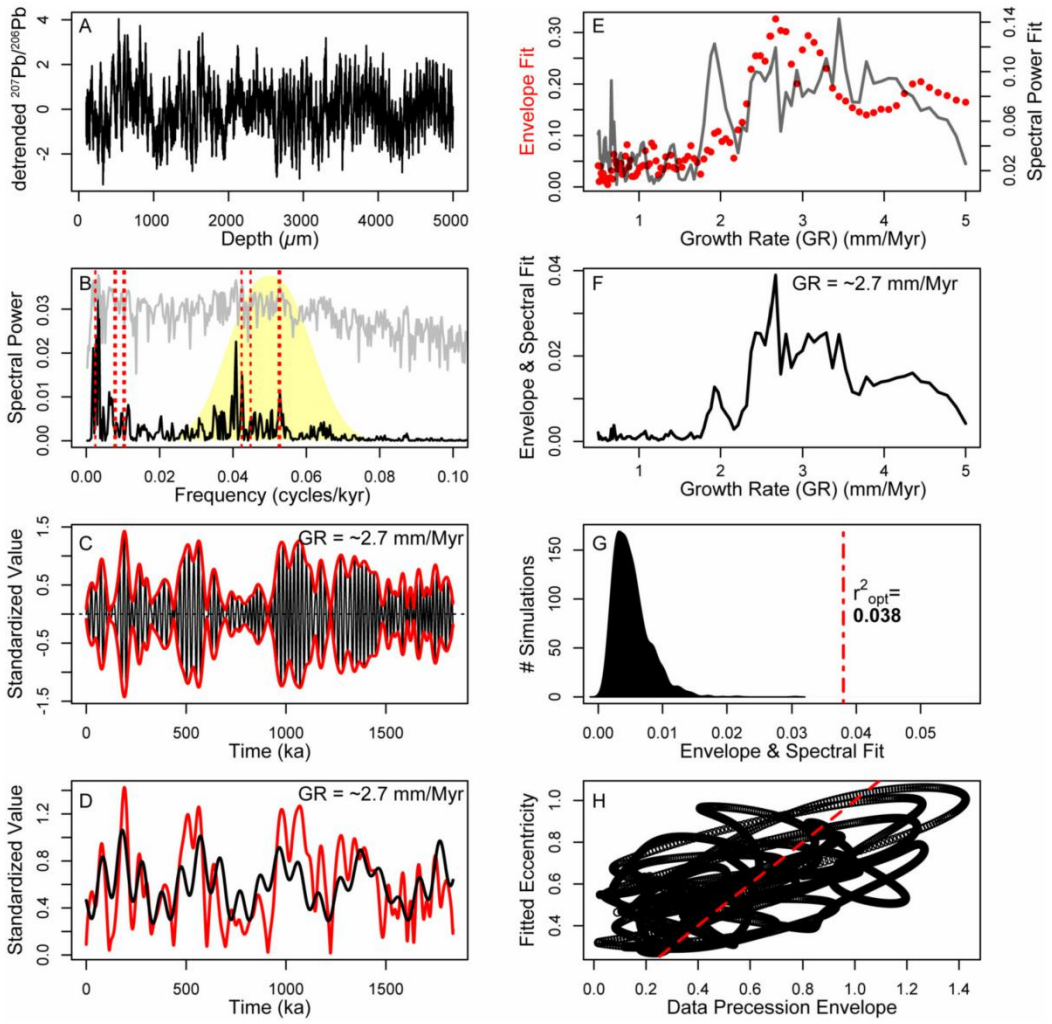

Figure 3. TimeOpt analysis performed in Astrochron (Meyers, 2015). (A) $^{207}Pb/^{206}Pb$ processed using standard methods (see Methods) prior to cyclostratigraphic analysis. (B) Periodogram of the $^{207}Pb/^{206}Pb$ data, using the TimeOpt growth rate of 2.7 mm/Myr. Grey and black lines are log and linear spectra, respectively. Dashed red lines are the precession and eccentricity periods. Yellow shaded area in (B) has been used for band-pass filtering in (C), with instantaneous amplitude in red determined via Hilbert transform. (D) Amplitude of band-pass filtered $^{207}Pb/^{206}Pb$ (red) compared with eccentricity model reconstructed by TimeOpt (Meyers, 2015). (E) Growth rates versus resulting squared Person correlation coefficients for envelope fit (r2, red dots) and spectral power fit (r2, grey line), which are combined in (F). Highest r2 fit of 0.038 is at ~ 2.7 mm/Myr (rounded from 2.668 mm/Myr). (G)

Significance of maximum observed r2 (from F) based on 2000 Monte Carlo simulations with AR1 surrogates (ρ = 0.826), yielding a p value of 0.005 (i.e., reject null hypothesis at 99.5% confidence level). (H) Cross plot of the amplitude of band-pass filtered 207Pb/206Pb and of the TimeOpt eccentricity model. Red dashed line is the 1:1 line.

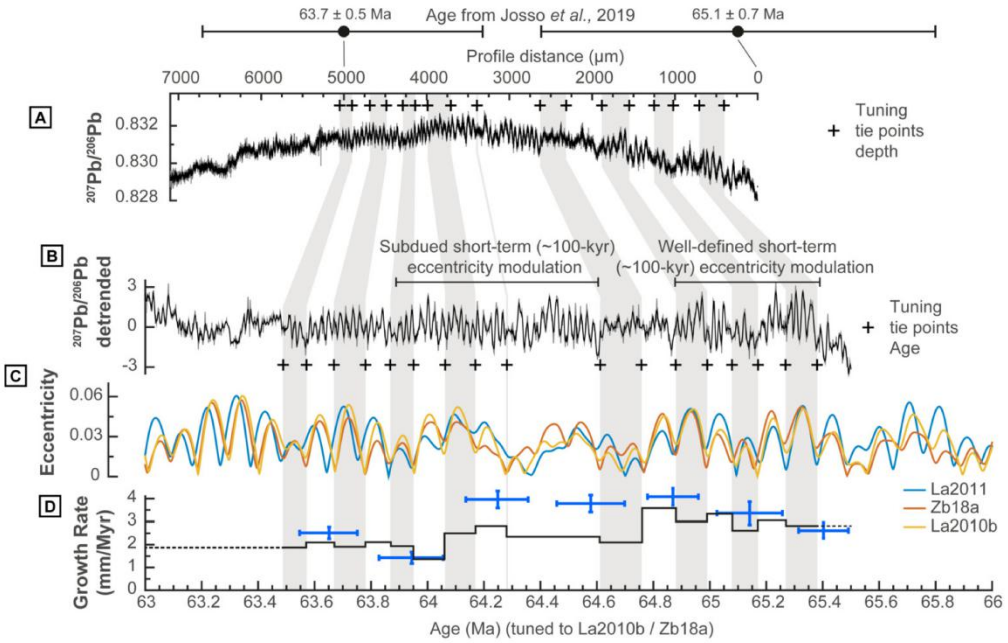

Figure 4. Astronomical tuning of the $^{207}Pb/^{206}Pb$ data. (A) Original $^{207}Pb/^{206}Pb$ isotope data (Fig. 2), with pluses denoting age correlation points and ages for profile distance d = 0 µm and d = 5000 µm from Josso et al. (2019). (B) Detrended and normalised $^{207}Pb/^{206}Pb$ data with equal age spacing (see Methods) to emphasise the cyclicity with pluses denoting tuning tie points. (C) Astronomical solutions of Earth's eccentricity: La2011 (Laskar et al., 2011), La2010b (Laskar et al., 2011), and Zb18a (Zeebe and Lourens, 2019). (D) Growth rates resulting from cyclostratigraphic analysis (black) and Co-chronometry data (±2σ , in blue) for this stratigraphic interval from Josso et al. (2019), notethe convergence in growth rate estimates between the two methods.

2. 全球硅酸盐风化通量过高估计

翻译人：蒋晓东 jiangxd@sustech.edu.cn

*Tipper E T, Stevenson E I, Alcock V, et al. G**lobal silicate weathering flux overestimated because of sediment－water cation exchange** [J]. PNAS, 2020, 2021: e2016430118. https://doi.org/10.1073/pnas.2016430118/-/DCSupplemental*

摘要：河流携带溶解态和固态硅酸盐风化产物，这一过程消耗大气二氧化碳因而在地质历史期对气候变化具有重要的负向反馈作用。本研究发现在一些河流系统中，在反应性交换池中一些悬浮颗粒吸附在矿物表面，可使阳离子通量增加到 50%。河流水与交换池的化学性质指示了均衡的交换，并进一步为 Sr 同位素所支持。全球硅酸盐风化通量的计算基于河流中来自硅酸岩矿物的溶解态 Na^+，交换池中大量供应的非硅酸盐 Na^+流入沉积区，尤其进入到广泛海洋沉积物的流域或者流域中岩石伴随着盐溶液流体。通过比较河流沉积物交换池与河流水化学，本研究定量研究了这一交换。发现在一些河流区域，阳离子交换为河水提供了主要的 Na^+离子，这对降低硅酸盐风化量的估算具有重要意义。本研究发现，硅酸盐风化通量在全球尺度上过高估算了 12%-28%。这一过高的估算量在快速剥蚀与沉积区极大，该区在负向气候反馈对化学风化反应具有极大的敏感性。近期其他的研究发现化学风化减少了二氧化碳的消耗量，大陆硅酸盐风化通量以及对地球二氧化碳排气通量的指示意义需要进一步研究。

ABSTRACT: Rivers carry the dissolved and solid products of silicate mineral weathering, a process that removes CO_2 from the atmosphere and provides a key negative climate feedback over geological timescales. Here we show that, in some river systems, a reactive exchange pool on river suspended particulate matter, bonded weakly to mineral surfaces, increases the mobile cation flux by 50%. The chemistry of both river waters and the exchange pool demonstrates exchange equilibrium, confirmed by Sr isotopes. Global silicate weathering fluxes are calculated based on riverine dissolved sodium (Na^+) from silicate minerals. The large exchange pool supplies Na^+ of nonsilicate origin to the dissolved load, especially in catchments with widespread marine

sediments, or where rocks have equilibrated with saline basement fluids. We quantify this by comparing the riverine sediment exchange pool and river water chemistry. In some basins, cation exchange could account for the majority of sodium in the river water, significantly reducing estimates of silicate weathering. At a global scale, we demonstrate that silicate weathering fluxes are overestimated by 12 to 28%. This overestimation is greatest in regions of high erosion and high sediment loads where the negative climate feedback has a maximum sensitivity to chemical weathering reactions. In the context of other recent findings that reduce the net CO_2 consumption through chemical weathering, the magnitude of the continental silicate weathering fluxes and its implications for solid Earth CO_2 degassing fluxes need to be further investigated.

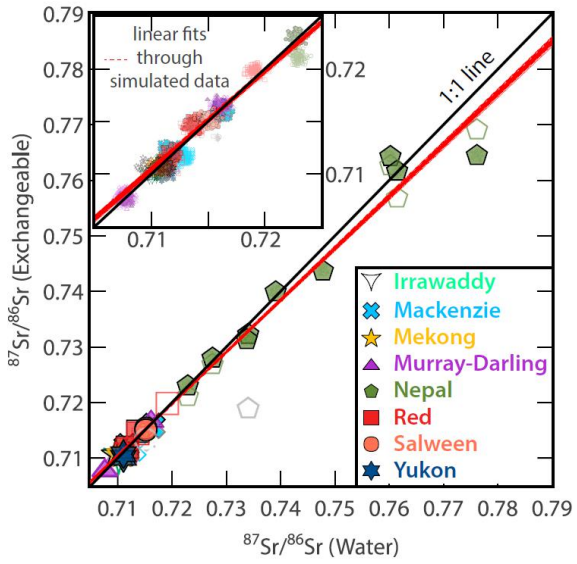

Figure 1. Sr isotope ratio in the exchange pool as a function of Sr isotopes in the river water. Open and closed (black outline) symbols used the NH_4Cl and CoHex methods, respectively. Gray symbols indicate samples where the water and exchange pool are not in equilibrium. Uncertainties (500 parts per million [ppm]) synthetically distributed about the mean of the data are illustrated by the small points (Inset). Red lines are 100 examples of linear fits through this synthetic CoHex data.

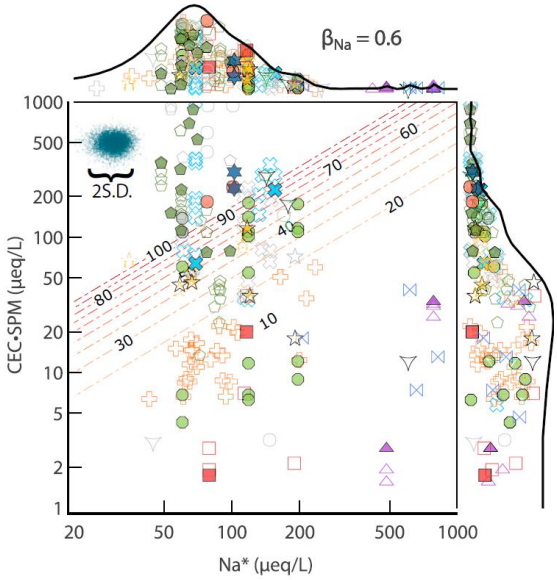

Figure 2. CEC.SPM vs. Na* contoured for the percentage reduction in silicate weathering flux 100. (Na*-Na_{sil})/Na* (0 = no change) calculated for ρNa = 0:6. Open and closed symbols used the NH_4Cl and CoHex methods, respectively. Gray symbols indicate water and exchange pool are not in equilibrium. Symbol legend is the same as for Fig. 2. Cluster of blue data points to indicate uncertainties are synthetic data distributed using the mean uncertainties of CEC.SPM and Na* determined using a Monte Carlo simulation. SI Appendix, Fig. S8 shows contours calculated for ρNa = 0:2.

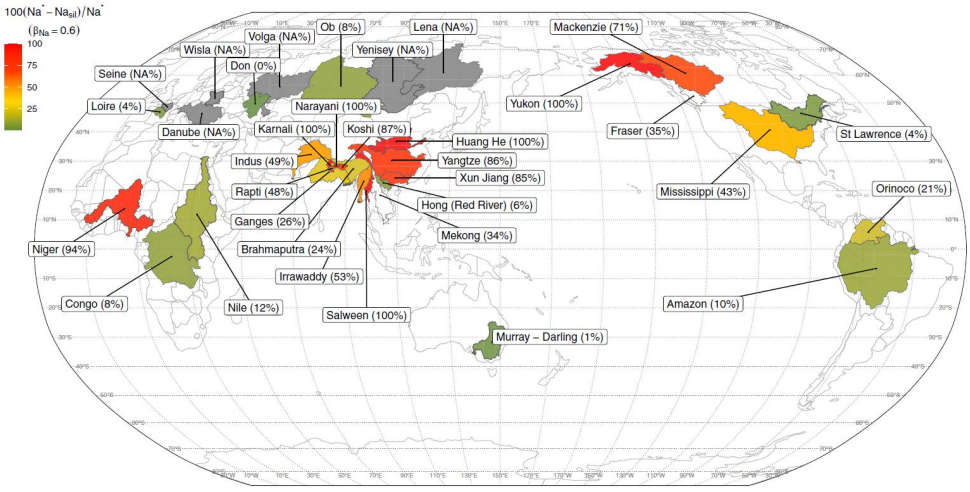

Figure 3. Global map of large river basins colored for percentage reduction in the silicate weathering flux (100. (Na*-Na_{sil}) = Na*) calculated for ρNa = 0.6 (SI Appendix, Fig. S8 is equivalent calculated for ρNa = 0.2). Basins in gray have chloride in excess of sodium (Na*<0).

3. 全球弧岩浆中的锂系统与地壳增厚对锂富集的重要性

翻译人：冯婉仪 fengwy@sustech.edu.cn

Chen C, Lee C T A, Tang M, et al. ***Lithium systematics in global arc magmas and the importance of crustal thickening for lithium enrichment****[J]. Nature communications, 2020,11:5313. https://doi.org/10.1038/s41467-020-19106-z*

摘要：世界上大部分 Li 矿床以盆地卤水的形式出现在岩浆造山带中，特别是在大陆火山弧中。然而，Li 在弧岩浆系统中富集的确切成因尚不清楚。在这里，我们展示了全球原始弧岩浆的 Li 含量和 Li/Y 比值与大洋中脊玄武岩的 Li 含量和 Li/Y 比值相似，说明俯冲板片对弧岩浆中 Li 富集的贡献有限。相反，我们发现弧下地幔熔融程度越低以及地壳内分异程度越高，Li 的富集程度越高。地壳较厚的弧更有利于这些富集效应，这就解释了为什么与岛弧相比，大陆弧（如：安第斯大陆弧）的岩浆作用和分异作用使得 Li 含量更高。这些富集的源岩经过风化作用将这些 Li 迁移到水文系统中，最终在加厚的造山背景下，由干旱气候和内陆伸展盆地结合发育成 Li 卤水。

ABSTRACT: Much of the world's Li deposits occurs as basinal brines in magmatic orogens, particularly in continental volcanic arcs. However, the exact origin of Li enrichment in arc magmatic systems is not clear. Here, we show that, globally, primitive arc magmas have Li contents and Li/Y ratios similar to mid-ocean ridge basalts, indicating that the subducting slab has limited contribution to Li enrichment in arc magmas. Instead, we find that Li enrichment is enhanced by lower degrees of sub-arc mantle melting and higher extents of intracrustal differentiation. These enrichment effects are favored in arcs with thick crust, which explains why magmatism and differentiation in continental arcs, like the Andes, reach greater Li contents than their island arc counterparts. Weathering of these enriched source rocks mobilizes and transports such Li into the hydrologic system, ultimately developing Li brines with the combination of arid climate and the presence of landlocked extensional basins in thickened orogenic settings.

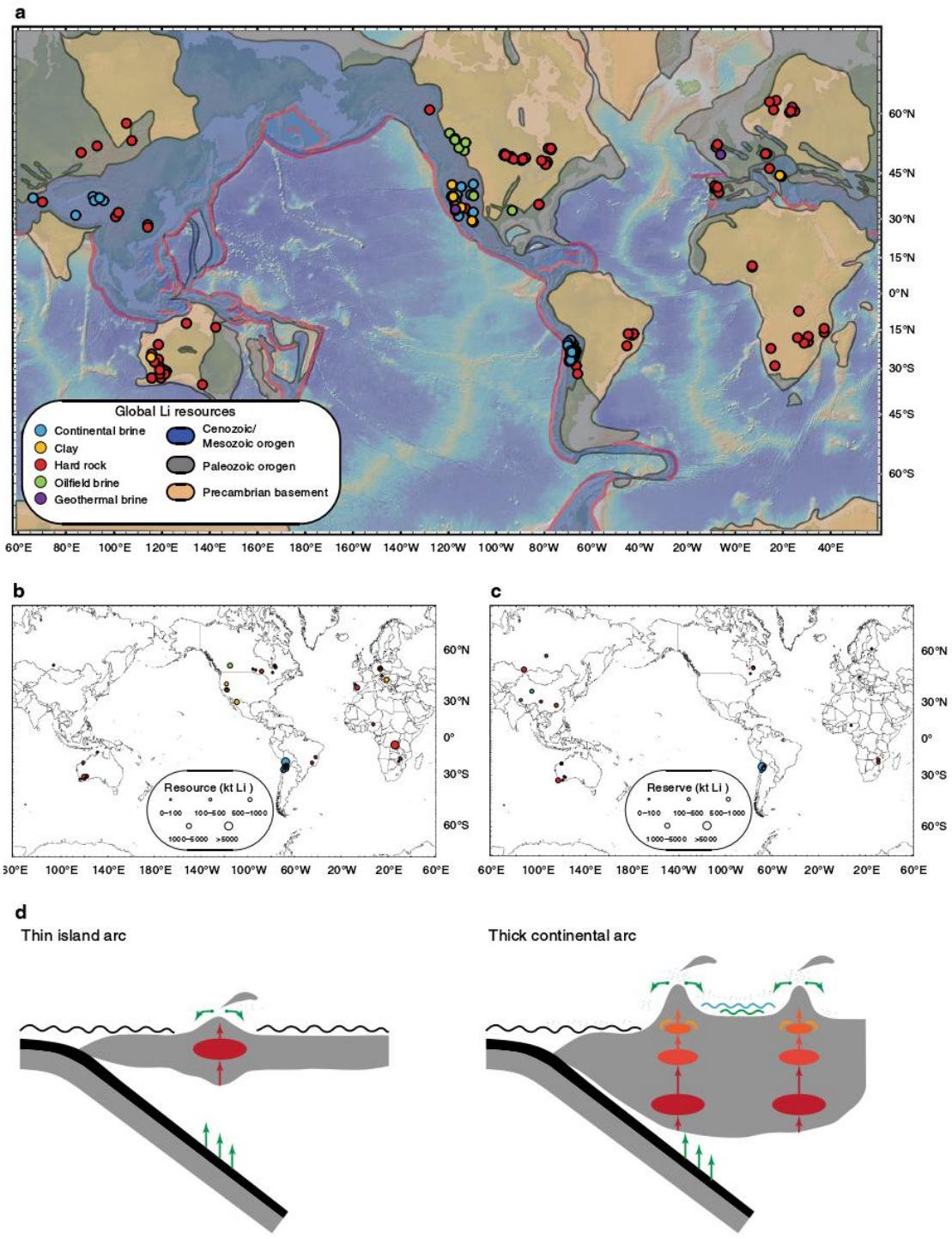

Figure 1. Distribution of global lithium deposits and conceptual cartoon describing Li cycling in subduction zones. a Map of continental brine, clay, pegmatite (hard rock), geothermal, and oilfield brine deposits based on compilations in this study (see Supplementary Dataset 1). Continental Li brines are dominantly found in Cenozoic/Mesozoic orogenic belts; pegmatites are found in eroded magmatic orogens (maps based on Roberts and Bally[59]). Base map was processed with GeoMapApp (http://www.geomapapp.org)[60]. b Map of estimated Li resources with size of symbols reflecting ktons

of Li metal. c Map of Li reserves with symbol size corresponding to ktons of Li metal. Resources represent the amount of available Li, whereas reserves represent that which can be extracted economically. Data are based on company reports compiled in this study (see Supplementary Dataset 1). d Conceptual model for Li cycling in subduction zones. Relative to background mid-ocean ridge basaltic volcanism, Li concentrations are enhanced in arc magmas by direct contributions from the subducting slab, melting in the mantle wedge, and fractional crystallization in the upper plate. Crystal fractionation is more extensive in thick continental arcs. In addition, mature continental arcs are often associated with net-evaporative intermontane basins. Weathering of andesitic and rhyolitic source rocks in thick continental arcs, followed by transport of solutes into these local basins, leads to further enrichment of Li. In island arcs, appropriate source rocks are scarce and any mobilized Li is likely lost to the ocean.

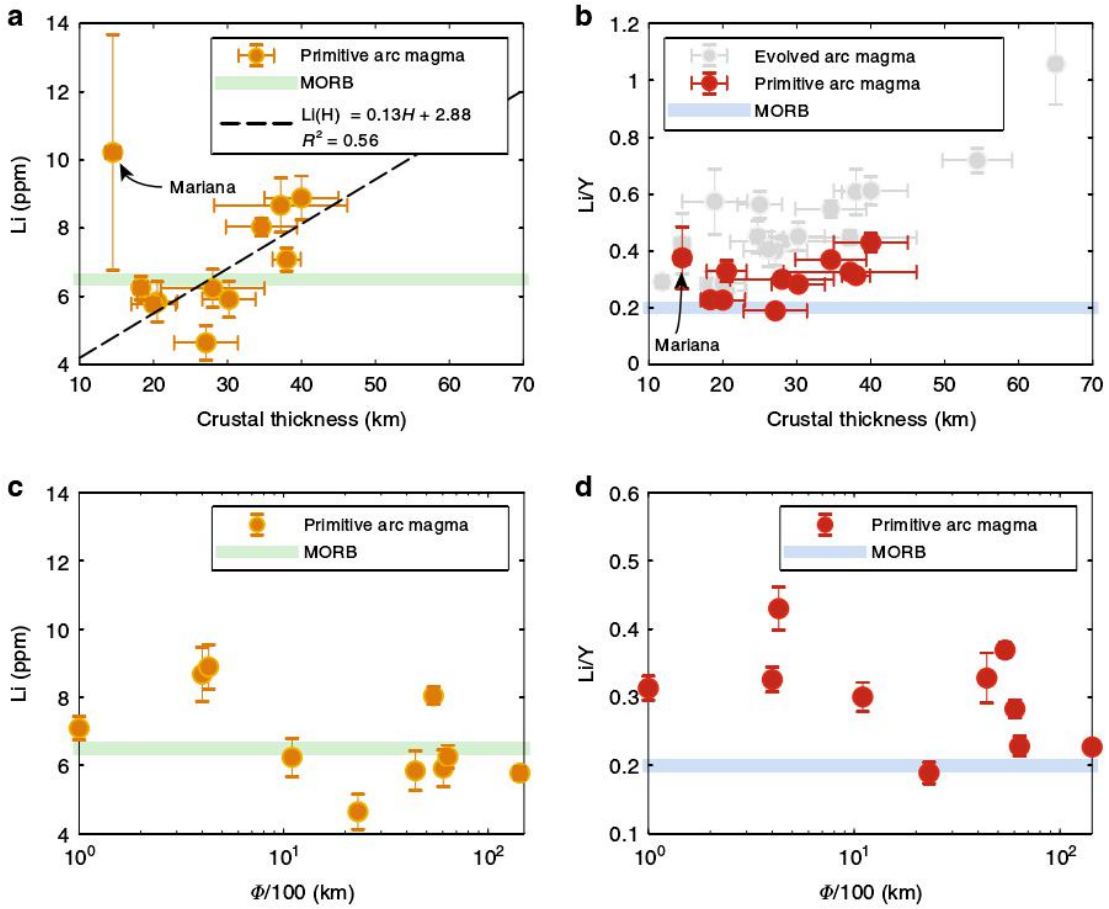

Figure 2. Li systematics of primitive arc magmas versus crustal thickness and slab thermal parameter. a, b Li and Li/Y in primitive arc magmas vs. crustal thickness. Primitive arc magmas represent only those with 48–52 wt.% SiO_2 and 6–15 wt.% MgO. In (b), dull gray symbols represent averages for more

evolved magmas (53–57 wt.% SiO_2). Error bars for Li concentration and Li/Y ratio are 2se; error bars for crustal thickness are one standard deviation (1σ) (Supplementary Dataset 2). As in Fig. 2, the pale green bar in (a and c) and blue bar in (b and d) show the average Li concentration of MORB from Gale et al.[22] and the Li/Y ratio of MORB from Ryan and Langmuir[9], respectively. The dashed line in (a) represents the linear regression of the data (with the Mariana arc excluded). c, d Li and Li/Y of primitive arc magmas vs. slab thermal parameter (Φ/100). Slab thermal parameters are from Syracuse et al.[34].

4. 南极洲 Ross sea 的 DSDP274 的新生代序列的磁性地层学

翻译人：李园洁 liyj3@sustech.edu.cn

Jovane L, Florindo F, Wilson G, et al. ***Magnetostratigraphic Chronology of a Cenozoic Sequence From DSDP Site 274, Ross Sea, Antarctica*** *[J]. Frontiers in Earth Science, 2020, 8:563453.*

https://doi.org/10.3389/feart.2020.563453

摘要：DSDP28 航次 274 孔的晚始新世-中中新世样品的新的古地磁结果可以为南极洲气候和冰盖演化的这个时期的古气候资料提供年代框架。基于新的年龄框架，晚始新世-中中新世沉积序列覆盖将近 20 Myr（~ 35 - ~ 15 Ma）。生物地层的约束与地磁极性年表相关。在距海底深度 260 m 之上的平均沉积速率 ~ 6 cm/kyr, 记录到一些间断面。260 mbsf 之下沉积速率接近 ~ 1 cm/kyr。在~ 180 mbsf 发现的一个不整合面占晚渐新世和早中新世至少 9 Myr 的时间，可能是南极洲极地洋流活动增强导致的不沉积和或侵蚀。在~ 180 mbsf 不整合面之上发现粒径和磁学性质发生剧烈波动，反映冰川前进和从大陆撤退的周期性行为。在南极洲边缘的其他钻孔的中新世序列中也识别到相似的冰川周期。

ABSTRACT： New paleomagnetic results from the late Eocene-Middle Miocene samples from Deep Sea Drilling Project Site 274, cored during Leg 28 on the continental rise off Victoria Land, Ross Sea, provide a chronostratigraphic framework for an existing paleoclimate archive during a key period of Antarctic climate and ice sheet evolution. Based on this new age model, the cored late Eocene-Middle Miocene sequence covers an interval of almost 20 Myr (from ~ 35 to ~ 15 Ma). Biostratigraphic constraints allow a number of possible correlations with the Geomagnetic Polarity Time Scale. Regardless of correlation, average interval sediment accumulation rates above 260 mbsf are ~ 6 cm/kyr with the record punctuated by a number of unconformities. Below 260 mbsf (across the Eocene/Oligocene boundary) interval, sedimentation accumulation rates are closer to ~ 1 cm/kyr. A major unconformity identified at ~180 mbsf represents at least 9 Myr

accounting for the late Oligocene and Early Miocene and represent non-deposition and/or erosion due to intensification of Antarctic Circumpolar Current activity. Significant fluctuations in grain size and magnetic properties observed above the unconformity at 180 mbsf, in the Early Miocene portion of this sedimentary record, reflect cyclical behavior in glacial advance and retreat from the continent. Similar glacial cyclicity has already been identified in other Miocene sequences recovered in drill cores from the Antarctic margin.

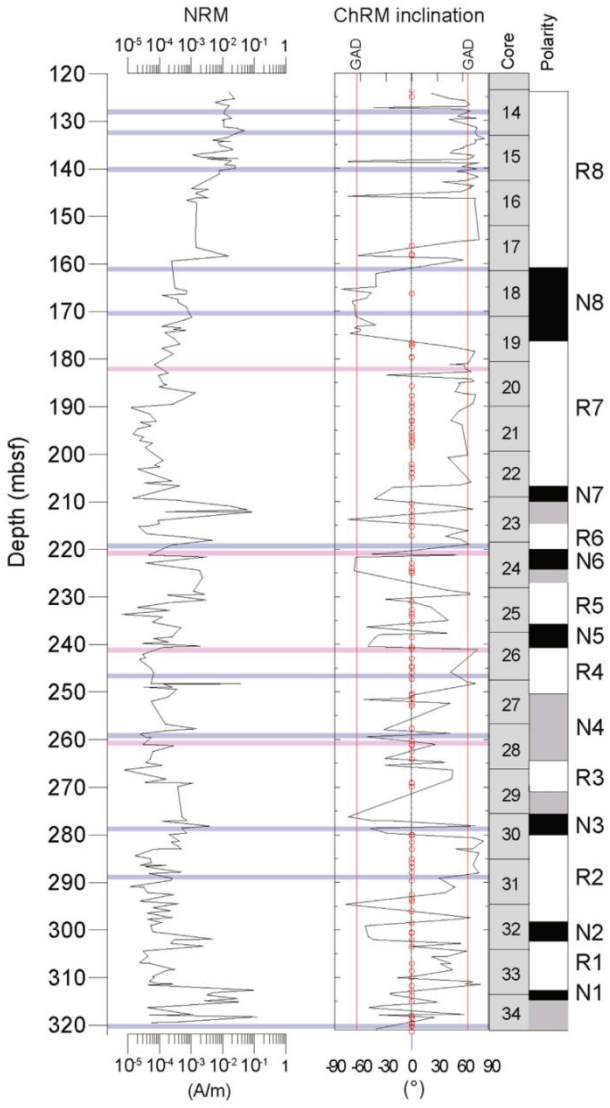

Figure 1. Downcore variations of NRM intensity, ChRM inclination, and magnetic polarity zonation (black denotes normal polarity and white denotes reversed polarity).

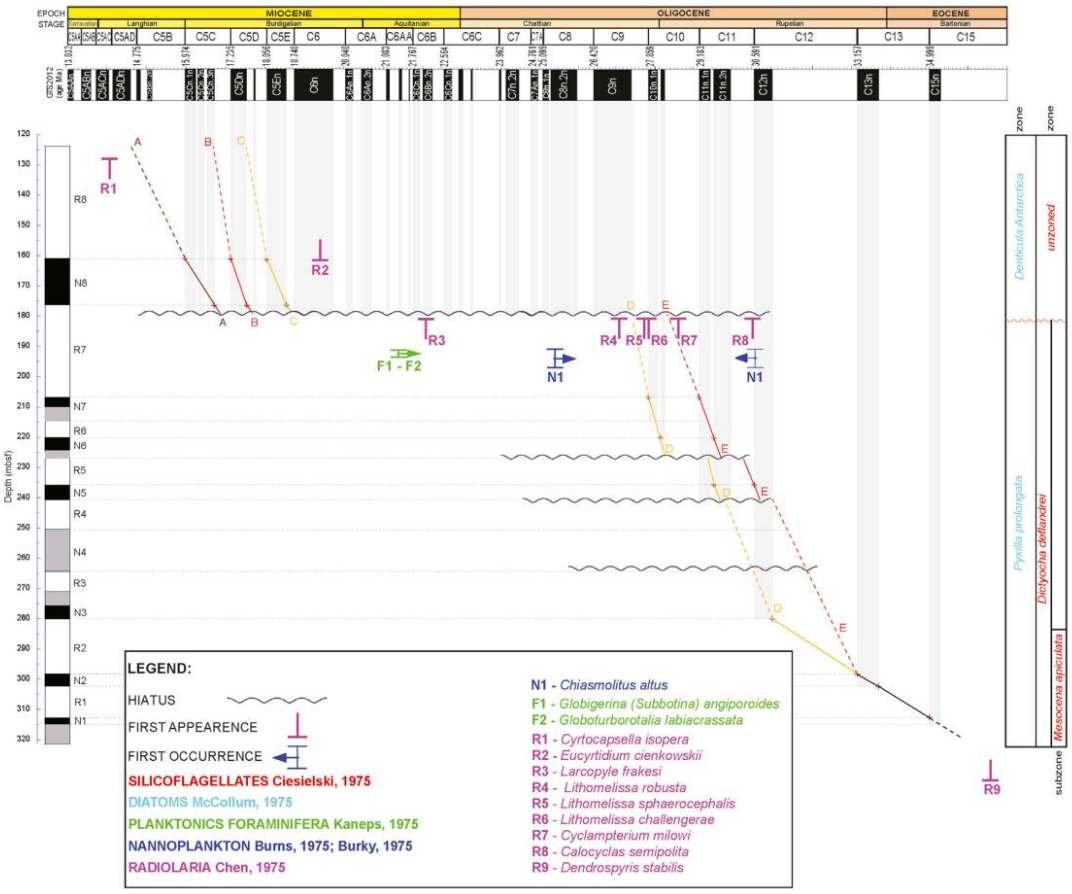

Figure 2. Age vs. depth plot with correlation of DSDP Site 274 polarity zonation to the GPTS of Gradstein et al. (2012). Hiatuses defined from the sedimentological data and biostratigraphical datum are represented following the legend. Magnetostratigraphic model A is in dark red; models B and E are in red; models C and D are in orange.

5. 南海神狐区域细粒沉积物粒度特征及其与天然气水合物饱和度的关系

翻译人：刘伟 inewway@163.com

He M , Zheng H , Clift P D. ***Zircon U－Pb geochronology and Hf isotope data from the Yangtze River sands: Implications for major magmatic events and crustal evolution in Central China*** *[J]. Chemical Geology, 2013, 360-361:186-203.*

https://doi.org/10.1016/j.chemgeo.2013.10.020

摘要：为了了解长江流域的地壳演化和历史，对从长江泥沙中分离出的碎屑锆石进行了原位U-Pb 和 Hf 同位素分析。采用 LA-ICP-MS U-Pb 分析，对 2277 颗碎屑锆石进行了定年，并对 674 颗碎屑进行了 Hf 同位素分析。结果表明，该盆地的 U-Pb 年龄主要分布在 2.4 - 2.6 Ga、1.8 - 2.0 Ga、700 - 850 Ma、400 - 550 Ma 和 200 - 300 Ma，与已知的吕梁期、晋宁期、加里东期、海西期和印支-燕山期花岗岩类岩浆事件相对应。锆石的初始 Hf 同位素比值[εHf(t)]在 5 个主要年龄群中均呈现出从负到正的大范围变化，揭示了在这些时期存在的地壳物质与不同体积的新地幔熔体混合在一起。锆石 Hf 模式年龄(TDM2)显示了两个主要的地壳生长范围，一个是中元古代（1.0 - 1.5 Ga），另一个是太古代-古元古代（2.5 - 2.8 Ga）。这些锆石主要来自扬子克拉通和华夏地块。基于 TDM2 模型的地壳生长速率显示，现今地壳体积的 30%在 2.5 Ga 形成，48%在 1.8 Ga 形成，70%在 1.4 Ga 形成，96%由 1.0 Ga 形成。

ABSTRACT: In situ U–Pb and Hf isotope analyses were made on detrital zircons isolated from sands of the Yangtze River in order to understand the evolution and history of crust in that river basin. A total of 2277 detrital zircon grains were dated by the LA-ICP-MS U–Pb technique and 674 grains were also analyzed for Hf isotopes on the same spots of concordant grains. Our results show five major groups of U–Pb ages: at 2.4–2.6 Ga, 1.8–2.0 Ga, 700–850 Ma, 400–550 Ma and 200–300 Ma, which correspond to known granitoid magmatic events within the drainage (Lüliangian, Jinningian, Caledonian, Hercynian and Indo-Sinian/Yanshanian). The initial Hf isotope ratios [εHf(t)] of the zircons exhibit a wide range from negative to positive for each of the five major age groups, revealing that existing crustal materials were mixing with variable volumes

of new mantle melt at these times. Zircon Hf model ages (TDM2) display two major ranges of crustal growth, one being Mesoproterozoic (1.0–1.5 Ga) and the other Archean–Paleoproterozoic (2.5–2.8 Ga). These zircons were mainly sourced from the Yangtze Craton and the Cathaysia Block, respectively. Crustal growth rates based on TDM2 model ages suggest that 30% of the present crustal volume was formed by 2.5 Ga, 48% by 1.8 Ga, 70% by 1.4 Ga and 96% was formed by 1.0 Ga.

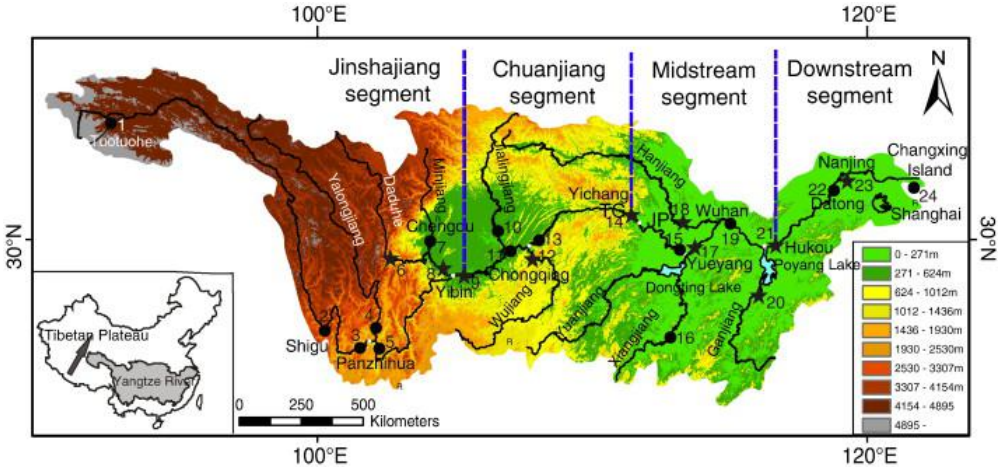

Figure 1. Landscape of the Yangtze River drainage basin shown as a shaded topographic map together with the sample locations. The Yangtze River is divided into four parts: the Jinshajiang, Chuanjiang, Midstream and Downstream segments. Circles indicate samples with zircons analyzed by U–Pb dating; Stars indicate samples with zircons dated by U–Pb dating and also analyzed for Hf isotopes. TG = Three Gorges, JP = Jianghan Plain.

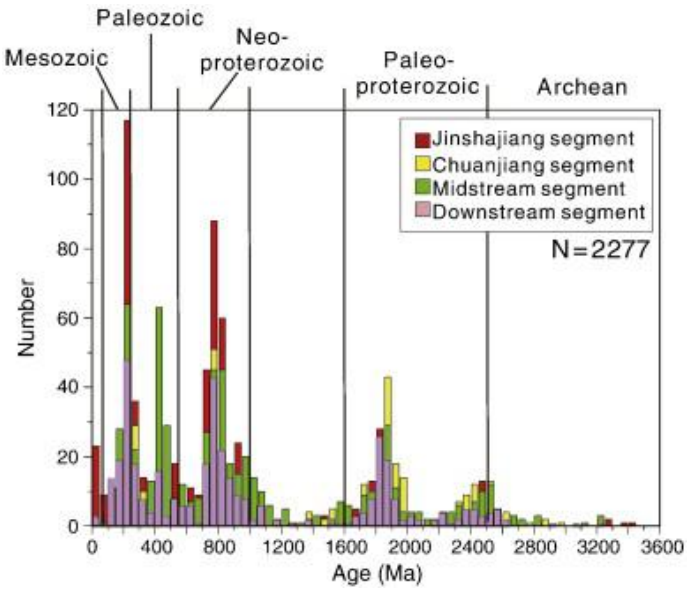

Figure 2. U–Pb age spectrum for the whole Yangtze River. Five major age peaks are observed at 2.4–2.6 Ga, 1.8–2.0 Ga, 700–850 Ma, 400–550 Ma and 200–300 Ma.

6. 我们能用地球的轴向磁偶极子场强度来预测反转吗？

翻译人：曹伟 11930854@QQ.com

Gwirtz K, Morzfeld M, Fournier A, et al. ***Can one use Earth's magnetic axial dipole field intensity to predict reversals?*** *[J]. Geophysical Journal International. 2020, online. https://doi.org/10.1093/gji/ggaa542*

摘要：我们的研究是仅通过偶极子强度来预测地球轴向磁偶极子场的反转。预测策略大致上是，一旦偶极子强度下降到阈值以下，那么磁场将继续减小，反转（或重大偏移）将发生。我们首先给出了一个基于强度阈值的预测策略的严格定义，然后描述了一个数学和数值框架来研究它在数据有限的情况下的有效性和适用性。我们将基于阈值的预测应用到数值模型的层次结构中，范围从简单的标量模型到三维地磁发电机。我们发现基于阈值的预测效果在模型层次结构中是不同的。效果上的差异可以用倒转如何发生的差异来解释：如果磁场朝着反转方向缓慢地减少（在本文中精确地说），预测效果就好；如果磁场迅速减少，预测水平就低。这种性质可以用作确定哪些模型符合类地模型的附加标准。将基于阈值的预测应用于过去 200 万年的 Virtual Axial Dipole Moment（VADM）古地磁重建（PADM2M 和 Sint-2000），揭示了一种基于阈值的地磁发电机预测技术。除了所有的局限性之外，基于阈值的预测表明，在未来 10 kyr 内不会出现逆转。然而，最重要的是，我们表明，考虑强度阈值来识别即将到来的反转本质上受到地球磁场动态行为的限制。

ABSTRACT: We study predictions of reversals of Earth's axial magnetic dipole field that are based solely on the dipole's intensity. The prediction strategy is, roughly, that once the dipole intensity drops below a threshold, then the field will continue to decrease and a reversal (or a major excursion) will occur. We first present a rigorous definition of an intensity threshold-based prediction strategy and then describe a mathematical and numerical framework to investigate its validity and robustness in view of the data being limited. We apply threshold-based predictions to a hierarchy of numerical models, ranging from simple scalar models to 3D geodynamos. We find that the skill of threshold-based predictions varies across the model hierarchy. The differences in

skill can be explained by differences in how reversals occur: if the field decreases towards a reversal slowly (in a sense made precise in this paper), the skill is high, and if the field decreases quickly, the skill is low. Such a property could be used as an additional criterion to identify which models qualify as Earth-like. Applying threshold-based predictions to Virtual Axial Dipole Moment (VADM) paleomagnetic reconstructions (PADM2M and Sint-2000) covering the last two million years, reveals a moderate skill of threshold-based predictions for Earth s dynamo. Besides all of their limitations, threshold-based predictions suggests that no reversal is to be expected within the next 10 kyr. Most importantly, however, we show that considering an intensity threshold for identifying upcoming reversals is intrinsically limited by the dynamic behavior of Earth's magnetic field.

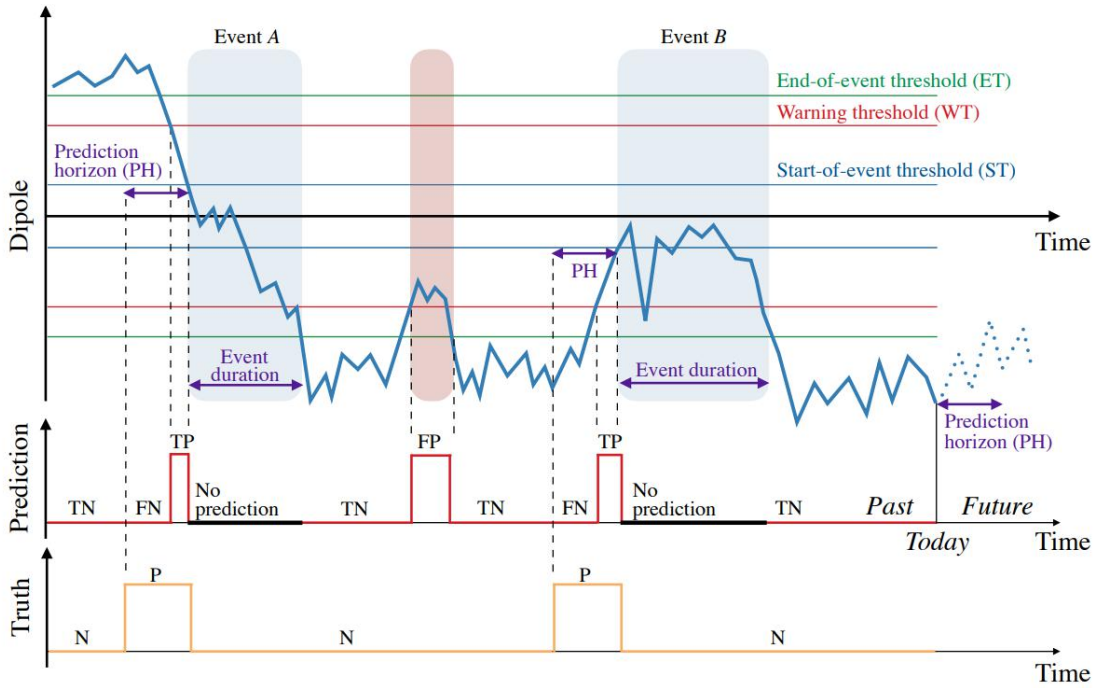

Figure 1. Illustration of the prediction strategy. Top: dipole (solid blue) as a function of time. The thin blue, green and red horizontal lines represent the start-of-event, the end-of-event and the warning thresholds. Two low-dipole events are labeled A (reversal) and B (excursion), and we indicate their event durations. Highlighted in red is a period of low intensity, which is not a low-dipole event, but where the low intensity causes false positives (FP). Towards the right, we illustrate a prediction over a given prediction horizon, which will lead to true negatives (TN). The prediction horizon also defines the true labels, (see bottom panel). Center : prediction as a function of time. The red line at zero

corresponds to the prediction no low-dipole event occurs during the prediction horizon, and the red line at one corresponds to the prediction a low-dipole event occurs during the prediction horizon. The thick black line segments correspond to periods during which no prediction is made. For events A and B, we first observe TNs, followed by false negatives (FN), caused by the warning threshold being small; then we observe TPs followed by a period during which no prediction is made. Bottom: true occurrences of low-dipole events within the prediction horizon. The orange line at zero corresponds to negatives (N), i.e., no low-dipole event occurs during the prediction horizon. The orange line at one corresponds to positives (P), i.e., a low-dipole event occurs during the prediction horizon.

7. 早渐新世冰川作用与东赤道太平洋生产力:对全球碳循环的启示

翻译人：王敦繁 dunfan-W@foxmail.com

Coxall H K, Wilson P A. ***Early Oligocene glaciation and productivity in the eastern equatorial Pacific: Insights into global carbon cycling*** *[J]. Paleoceanography, 2011, 26: PA2221. https://doi.org/10.1029/2010PA002021*

摘要：南极始新世-渐新世转换（EOT）期间持续冰期的开始标志着地球气候的一个关键变化，但我们对这一事件尤其是碳循环的作用认识有限。为了解决这个问题我们通过对赤道东太平洋 1218 钻孔古海洋指标进行了解读：(1) 底栖有孔虫碳氧同位素记录支持以前的的记录；(2) 浅栖有孔虫 *Oridorsalis umbonatus* 的碳氧同位素记录以及 (3) 底栖有孔虫积累速率记录。我们新的同位素数据验证了 1218 孔$\delta^{18}O$ 存在两阶段增加。BFAR 的记录表明，在南极冰期开始时，相对于渐新世 BFAR 出现了一个短暂的（约 500 kyr）峰值，该峰值为两到三倍，可能是因为 EEP 中生物出口产量的增加。这与南大洋蛋白石积累的历史具有相同的一般形式，表明了强烈的高纬度-低纬度海洋耦合。矛盾的是，EEP 地区早渐新世沉积物的有机碳埋藏非常差，而大气中二氧化碳分压的代用记录表明，EOT 与大气中二氧化碳分压的短暂增加有关。

ABSTRACT: The onset of sustained Antarctic glaciation across the Eocene-Oligocene transition (EOT) marks a pivotal change in Earth's climate, but our understanding of this event, particularly the role of the carbon cycle, is limited. To help address this gap we present the following paleoceanographic proxy records from Ocean Drilling Program Site 1218 in the eastern equatorial Pacific (EEP): (1) stable isotope ($\delta^{18}O$ and $\delta^{13}C$) records generated in epifaunal benthic foraminifera (*Cibicidoides* spp.) to improve (double the resolution) the previously published records; (2) $\delta^{18}O$ and $\delta^{13}C$ records measured on *Oridorsalis umbonatus*, a shallow infaunal species; and (3) a record of benthic foraminifera accumulation rate (BFAR). Our new isotope data sets confirm the existence at Site 1218 of a two-step $\delta^{18}O$ increase. They also lend support to the hypothesized existence of a late Eocene transient $\delta^{18}O$ increase and early Oligocene Oi-1a and

Oi-1b glacial maxima. Our record of BFAR indicates a transient (~500 kyr) twofold to threefold peak relative to baseline Oligocene values associated with the onset of Antarctic glaciation that we attribute to enhanced biological export production in the EEP. This takes the same general form as the history of opal accumulation in the Southern Ocean, suggesting strong high-to-low-latitude oceanic coupling. These findings appear to lend support to the idea that the EOT $\delta^{13}C$ excursion is traceable to increased organic carbon (C_{org}) burial. Paradoxically, early Oligocene sediments in the EEP are extremely C_{org}-poor, and proxy records of atmospheric pCO_2 indicate a transient increase associated with the EOT.

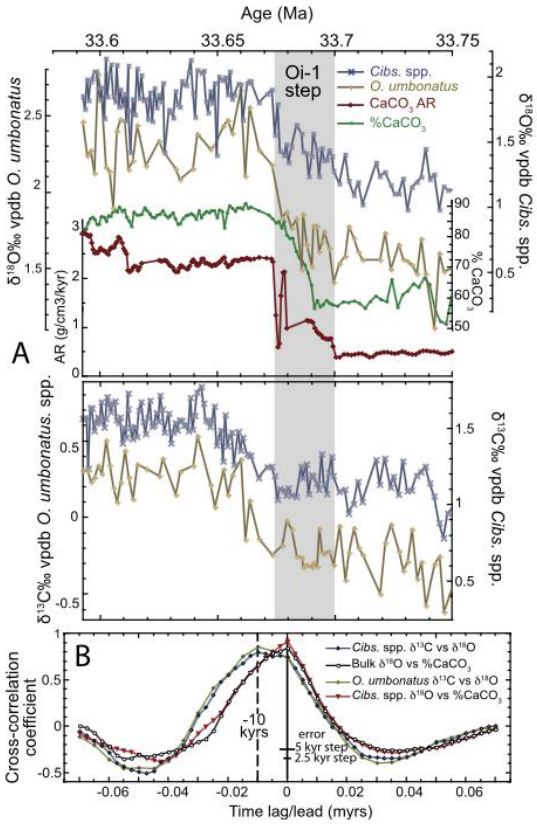

Figure 1. Analysis of climate proxy leads and lags across the Oi-1 isotopic step. (a) Close-up of Site 1218 benthic $\delta^{18}O$, $\delta^{13}C$, and bulk sediment weight $\%CaCO_3$ between 33.59 and 33.75 Ma showing the timing of geochemical changes across Oi-1. (b) Cross-correlations of benthic $\delta^{18}O$ and $\delta^{13}C$, bulk sediment $\delta^{18}O$, and bulk $\%CaCO_3$ as individual pairs for the Oi-1 interval. The *Cibicidoides* spp. and O. *umbonatus* records suggest that benthic $\delta^{13}C$ lags $\delta^{18}O$ by ~10 kyr across Step 2 whereas $\%CaCO_3$ and $\delta^{18}O$ (all species) are in phase (see Table 2 for correlation statistics). Errors are equal to plus or minus half time step. Site 1218 bulk $\delta^{18}O$ is from Pälike et al. [2006].

8. 青藏高原是如何动态影响夏季季风降水的?

翻译人：杨会会 11849590@mail.sustech.edu.cn

Son J H, Seo K H, Wang B. ***How does the Tibetan Plateau dynamically affect downstream monsoon precipitation?****[J].Geophysical Research Letters, 2020, 2020GL090543.*
https://doi.org/10.1029/2020GL090543

摘要：最近的研究表明，机械效应对东亚夏季风（EASM）的影响要大于热力效应。然而，其潜在动力机制的理论基础尚未阐明。之前的研究表明，地形强迫正压Rossby波理论很好地解释了季风降水的季节演变及其幅度和峰值位置。侵袭西藏的副热带纬向风高原是一个关键因素，由此产生的下游气旋性环流异常和反气旋性环流异常在两者之间形成一个纬向位势高度梯度峰值，导致经向风的发展，并伴随水汽输送到东亚季风区。随着季节接近夏季季风期，峰顶位势高度梯度—即季风雨带—从西北太平洋向西转移到东亚。本研究成果可应用于全球亚热带季风。

ABSTRACT: Recent studies have demonstrated that mechanical effects have a greater contribution to the East Asian summer monsoon (EASM) than thermodynamical effects. However, a theoretical basis for the underlying dynamical mechanism has not been elucidated. The present study shows that topographically forced barotropic Rossby wave theory well explains the seasonal evolution of the monsoonal precipitation and its amplitude and peak location. The subtropical zonal wind impinging on the Tibetan Plateau is a key factor, and the resulting downstream cyclonic and anticyclonic circulation anomalies form a peak zonal geopotential height gradient in between, leading to the development of the meridional wind and the accompanying moisture transport to the EASM region. As the season approaches the summer monsoon period, the peak geopotential height gradient – thus the monsoonal rainband – shifts to the west from the western North Pacific to East Asia. The findings in this study can be applied to subtropical monsoons worldwide.

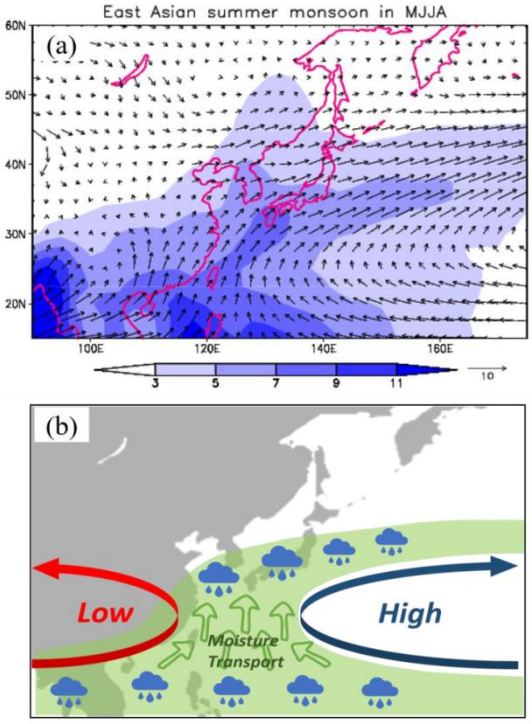

Figure 1. Characteristics of the East Asian summer monsoon (EASM). (a) Climatological mean precipitation and horizontal wind at 850 hPa in boreal summer (May to August), and (b) schematic of the EASM.

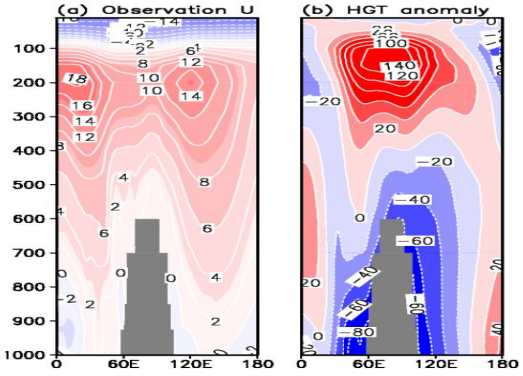

Figure 2. Vertical structure of the atmosphere around the Tibetan Plateau. Vertical and zonal cross-section of (a) zonal wind (m s^{-1}) and (b) geopotential height (m), averaged over 25°–35°N during May–August. The geopotential height anomaly is calculated by deviations from the zonal average at each pressure level.

9. 全新世亚洲季风与稳定水同位素的轨道驱动：模型与实测结果对比

翻译人：李海 12031330@mail.sustech.edu.cn

Tharammal T, Bala G, Paul A, et al. ***Orbitally driven evolution of Asian monsoon and stable water isotope ratios during the Holocene: Isotope-enabled climate model simulations and proxy data comparisons*** *[J]. Quaternary Science Reviews, 2021, 252: 106743.*

https://doi.org/10.1016/j.quascirev.2020.106743

摘要：稳定水同位素是理解全新世以来南亚季风区降水变化的重要气候指标。本次研究，利用同位素气候模型探究全新世早期以来（8 ka）南亚地区降水中水同位素对轨道变化的响应。8 - 4 ka降水随着夏季日照增加而增加，模拟结果显示$\delta^{18}O_{precip}$的负比值也相应增加。模型显示南亚地区$\delta^{18}O_{precip}$最湿润期和$\delta^{18}O_{precip}$最大损耗期为8 ka。我们发现环流的增强、对流增加和降水将会导致南亚地区$\delta^{18}O_{precip}$的减少。在以对流降水为主的印度季风区，$\delta^{18}O_{precip}$值与对流、降水呈负相关。东亚地区$\delta^{18}O_{precip}$值与区域降水相关性较差，可能与上游地区对流增强、水汽分散和混合降水类型有关。根据代用指标推断出的$\delta^{18}O$值对$\delta^{18}O_{precip}$模型值进行评估。代用指标记录与模拟结果在4 ka、6 ka、和8 ka一致，2 ka阶段的模拟结果与某些地区的记录不一致。

ABSTRACT: The variation of stable water isotopes ($\delta^{18}O$, δD) in climate archives is an important proxy to understand the evolution of South Asian monsoon (SA) precipitation over the Holocene. In this study, using an isotope-enabled climate-model, we examine the responses of water isotopes in precipitation over the SA region to orbital changes in the early to late Holocene (8 ka to 0 ka). Precipitation is enhanced during 8 ka to 4 ka in response to increased summertime insolation, and correspondingly, larger magnitudes of negative water isotope ratios in precipitation ($\delta^{18}O_{precip}$) are simulated. The model-simulated wettest period and the corresponding period of maximum depletion of $\delta^{18}O_{precip}$ in the SA region is the 8 ka period. We find that strengthened circulation, increased convection, and precipitation led to the $\delta^{18}O_{precip}$ depletion in the SA region. In the

tropical Indian monsoon region, where convective precipitation is dominant, the $\delta^{18}O_{precip}$ values are inversely correlated with the local convection and the amount of precipitation. The $\delta^{18}O_{precip}$ values in the East Asian Summer Monsoon (EASM) region are not well-correlated with local precipitation, likely due to the enhanced convection and depletion of vapor in upstream areas and mixed precipitation types in the region. The modeled $\delta^{18}O_{precip}$ values are evaluated against $\delta^{18}O$ inferred from proxy archives. Proxy data and model-simulated isotope ratios in precipitation agree on the larger magnitude of negative isotopic values during the 4 ka, 6 ka, and 8 ka periods relative to the present, although model-simulated enrichment in the 2 ka period is inconsistent with some proxy-records.

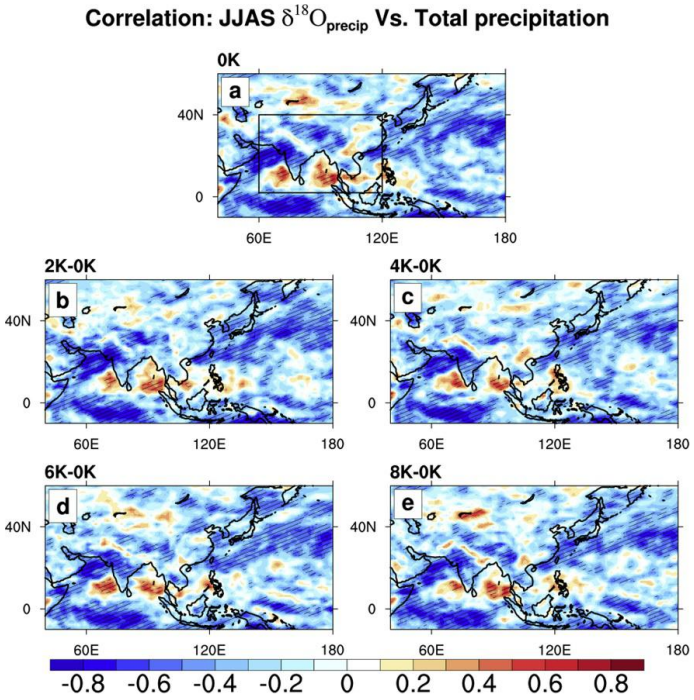

Figure 1. The correlation between JJAS mean $\delta^{18}O_{precip}$ in permil and amount of precipitation in mm day−1 in a) the 0K simulation and the correlation between the anomalies [b) 2K–0K, c) 4K–0K, d) 6K–0K, and e) 8K–0K] of $\delta^{18}O_{precip}$ and amount of precipitation.

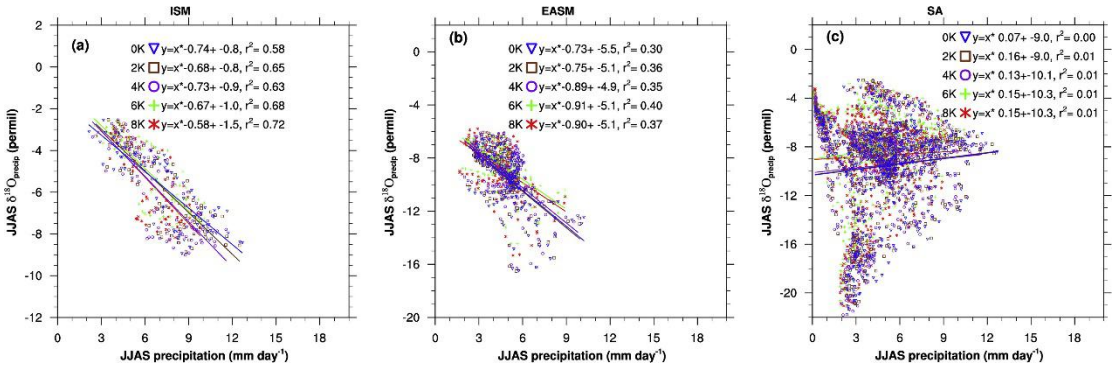

Figure 2. Linear relationship between JJAS mean $\delta^{18}O_{precip}$ (in permil) and precipitation (in mm day^{-1}) over the land regions for a) tropical (5°N-25°N, 60°E−95°E) ISM region, b) EASM region, and c) the SA region in the 0K, 2K, 4K, 6K, and 8K simulations. The regression, slope and r2 from the regression analysis are shown in the panels.

10. 伊朗中部 Garedu 组记录的侏罗纪板块漂移

翻译人：周洋 zhouy3@sustech.edu.cn

Mattei M, Muttoni G, Cifelli F. ***A record of the Jurassic massive plate shift from the Garedu Formation of central Iran*** *[J]. Geology, 2014, 42: 555–558.*

https:// doi:10.1130/G35467.1

摘要：现代的 APWPs 显示在中侏罗至晚侏罗世（175-145 Ma）期间，北美和非洲坐标系中极地位置发生快速的移动（板块漂移），文献中的其他曲线往往被低估了。北大西洋板块环线的欧亚大陆也发现了这种侏罗纪大规模极移（JMPS），具有广泛的古地理意义，但是来自该大陆的侏罗纪数据很少且有一些问题。本次研究，我们获得了来自伊朗的 Kimmeridgian–Tithonian（晚侏罗纪世）Garedu 组的古磁数据，Garedu 组自三叠纪以来就是欧亚大陆的一部分。古磁性显示沉积的古纬度与结合了 JMPS 的 APWPs 预测的伊朗纬度降低一致。此外，我们根据这些 APWPs 计算出的古纬度，可以更好地解释中生代期间伊朗的整体地层的演化。当伊朗从三叠纪晚期的热带干旱带向中纬度湿润带漂移时，碳酸盐台地生产力停止，开始接收广泛的含煤的沉积；当伊朗在 JMPS 期间回到干旱热带纬度时，碳酸盐台地生产力和蒸发相沉积重新恢复。这些结果说明（1）强有力的但通常被忽视的跨区域气候带控制的板块运动（大陆漂移或极地漂移）影响了沉积相；（2）精确控制古地理重建对于构造解释的重要性，尤其是在侏罗纪等板块快速运动时期。对未来研究的建议，我们预测采用包含 JMPS 的欧亚参考古地磁极可能会导致关于中亚变形历史的现有地质和古磁数据的重新解释。

ABSTRACT: Modern generations of apparent polar wander paths (APWPs) show the occurrence in North American and African coordinates of a major and rapid shift in pole position (plate shift) during the Middle to Late Jurassic (175–145 Ma) that alternative curves from the literature tend to underestimate. This Jurassic massive polar shift (JMPS), of vast and as-yet unexplored paleogeographic implications, is also predicted for Eurasia from the North Atlantic plate circuit, but Jurassic data from this continent are scanty and problematic. Here we present paleomagnetic

data from the Kimmeridgian–Tithonian (upper Jurassic) Garedu Formation of Iran, which was part of Eurasia since the Triassic. Paleomagnetic component directions of primary (pre-folding) age indicate a paleolatitude of deposition that is in excellent agreement with the latitude drop predicted for Iran from APWPs incorporating the JMPS. Moreover, we show that paleolatitudes calculated from these APWPs, used in conjunction with simple zonal climate belts, better explain the overall stratigraphic evolution of Iran during the Mesozoic. As Iran drifted from the tropical arid belt to the mid-latitude humid belt in the Late Triassic, carbonate platform productivity stopped while widespread coal-bearing sedimentation started, whereas as Iran returned to arid tropical latitudes during the JMPS, carbonate platform productivity and evaporitic sedimentation resumed. These results illustrate (1) the potent, but often neglected, control that plate motion (continental drift and/or true polar wander) across zonal climate belts exerts on the genesis of sedimentary facies; and (2) the importance of precisely controlled paleogeographic reconstructions for tectonic interpretations, especially during times of fast plate motion like the Jurassic. As a suggestion for future research, we predict that the adoption of Eurasian reference paleopoles incorporating the JMPS may lead to a reconciliation (or reinterpretation) of existing geologic and paleomagnetic data regarding the deformation history of central Asia.

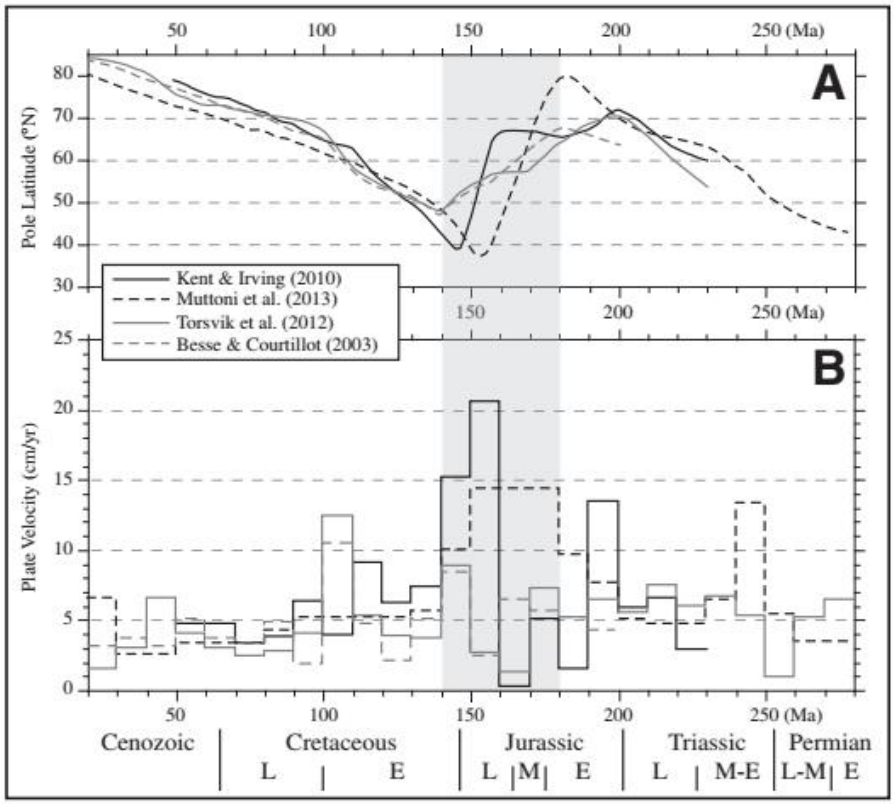

Figure 1. A: Latitudes of paleomagnetic poles from different apparent polar wander paths (APWPs) from the literature, in African coordinates; drop of pole latitude during Jurassic massive polar shift (JMPS; within gray vertical band) is evident in the Kent and Irving (2010) and Muttoni et al. (2013) APWPs. B:Velocity of African plate calculated from different APWPs; high plate velocity characterizes the JMPS, especially according to the Kent and Irving (2010) APWP. L—late; M—middle; E—early.

11. 利用磁化率通过普通协克里金法绘制城市污染点土壤铅浓度图

翻译人：张伟杰 12031188@mail.sustech.edu.cn

Golden N, Zhang C, Potito A, et al. ***Use of ordinary cokriging with magnetic susceptibility for mapping lead concentrations in soils of an urban contaminated site*** *[J]. Journal of Soils and Sediments, 2019, 20: 1357-1370.*

https://doi.org/10.1007/s11368-019-02537-7

摘要：铅污染是影响世界各地城市的普遍问题。传统的野外工作和实验室分析技术既费时又昂贵。本研究的目的是评价通过普通克里金方法（OK）进行协克里金插值（CK）在以体积磁化率（κ）作为污染城市土壤铅空间插值协变量时的插值效果。本研究的研究对象是之前未受管理的垃圾填埋场的受污染的城市土壤。采用间隔 20 m 的系统采样网格，共采集了 76 个地表样品（0 - 10 cm）。磁化率测量是在密度较高的 10 米间隔内进行的，共进行 288 次测量。因此，将其作为 CK 法预测 Pb 浓度的辅助变量，以改善 Pb 的空间插值。为了确定 CK 比普 OK 方法的有效，在插值之前降低样本的空间密度。随机选取约 15%、25%、35%、50% 的 Pb 样品进行验证。全房向变异函数和协方差在插值前使用对数转换数据拟合。Spearman's Rho 相关分析结果显示，κ与 Pb 浓度有显著相关性（$r_s = 0.676$, $p < 0.01$）。通过普通克里金方法进行的协克里金插值的有效性通过有效性验证数据验证。统计结果表明，在 CK 中使用 lnκ作为 lnPb 的辅助数据时，lnPb 的均方根误差(RMSE)总体较低，CK 程序预测的 lnPb 值与实测 lnPb 的 r2 值比 OK 更高。CK 法使用空间密度降低后的 49 个 Pb 点的模型更准确，RMSE 为 0.550, r2 为 0.730, $p < 0.01$。这项技术可以大大降低野外工作和土壤分析的成本。为了可以有效的进行 CK，Pb 和κ的测量值必须具有相当大的空间连续性。在适用的情况下，它可以用于特定地点的铅暴露对生态系统、人类健康或城市绿地内的水体、路边土壤、已分配或待重新开发的城市用地的危害。

ABSTRACT: Lead contamination is a prevalent issue affecting cities worldwide. Traditional fieldwork and laboratory analysis techniques can be time-consuming and costly. The purpose of this study was to evaluate the performance of ordinary cokriging (CK) when volume magnetic

susceptibility (κ) is used as a co-variable for spatial interpolation of Pb in contaminated urban soils. The study was conducted in contaminated urban soils of a former unregulated landfill site. A total of 76 surface samples (0–10 cm) were collected using a systematic sampling grid separated by 20-m intervals. Magnetic susceptibility measurements were taken at a higher density of 10-m intervals with 288 measurements. Thus, it was used as an auxiliary variable to predict Pb concentrations by the CK procedure with an aim to improve spatial interpolation of Pb. To determine the effectiveness of CK over the ordinary kriging (OK) procedure, the spatial density of samples was reduced prior to interpolation. A total of ~ 15%, 25%, 35%, and 50% of the Pb samples were randomly selected and reserved for validation. Omnidirectional semivariograms and covariograms were fitted using log-transformed data prior to interpolation. Measurements of κ shared a significant relationship with Pb concentrations by the Spearman's Rho correlation analysis ($r_s = 0.676$, $p < 0.01$). The effectiveness of the CK procedure over OK was determined using validation datasets. Statistically, the results showed that lnPb when its auxiliary relations with lnκ were used in CK had overall lower "root mean square error" (RMSE) and predicted lnPb values from the CK procedure had a higher r2 value with measured lnPb than OK. A model produced by the CK procedure with a reduced spatial density of 49 Pb points provided the more accurate map with a RMSE of 0.550 and an r^2 value of 0.730, $p < 0.01$ level. This technique can potentially reduce fieldwork and soil analysis costs considerably. Measurements of Pb and κ must share a substantial level of spatial continuity to implement CK effectively. Where applicable, it can be used in the site specific evaluation of hazard posed by Pb exposure to ecosystems, human health or water bodies in urban green spaces, roadside soils, allotments or brownfield sites.

Dataset type	R^2	RMSE	ME
(a) Ordinary kriging			
$lnPb_{-15\%}$	0.596	0.902	0.037
$lnPb_{-25\%}$	0.431	0.926	−0.185
$lnPb_{-35\%}$	0.359	1.258	0.293
$lnPb_{-50\%}$	0.332	0.952	−0.056
(b) Ordinary cokriging			
$lnPb_{-15\%}$	0.848	0.600	0.300
$lnPb_{-25\%}$	0.545	0.890	−0.093
$lnPb_{-35\%}$	0.730	0.550	0.090
$lnPb_{-50\%}$	0.622	0.765	−0.220

Table 1. Summary of prediction metrics for best performing (a) ordinary kriging and (b) ordinary cokriging models from each spatial density of Pb samples

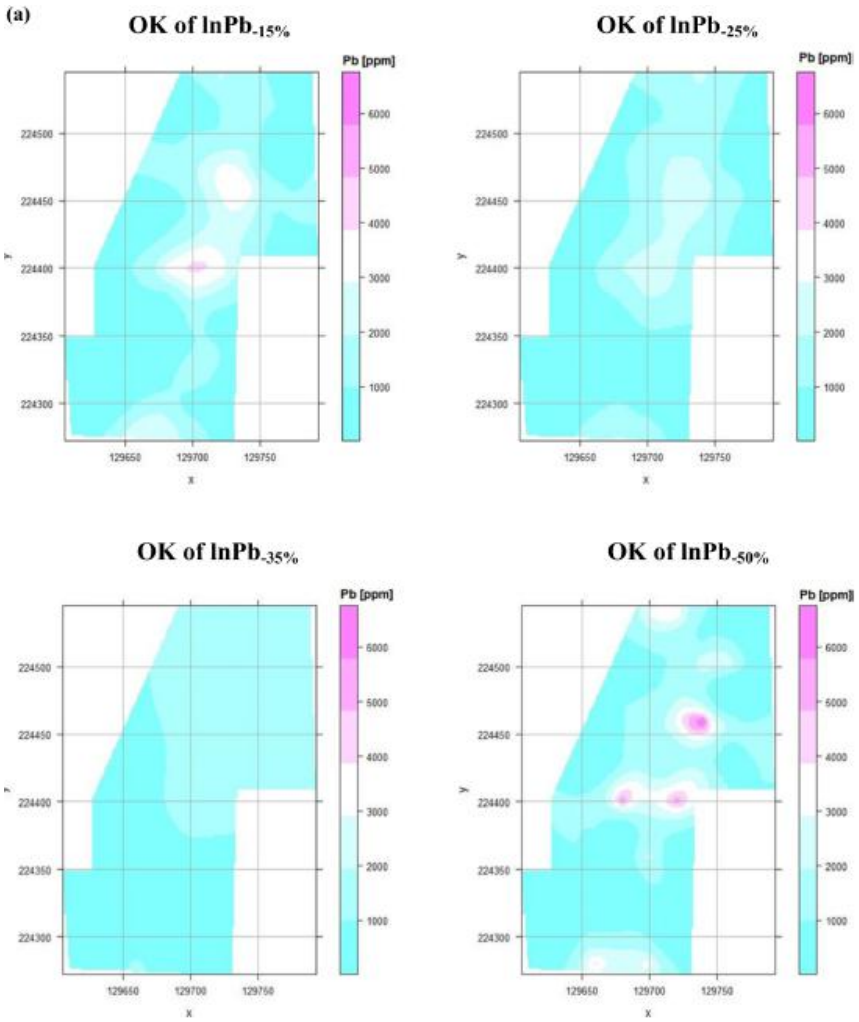

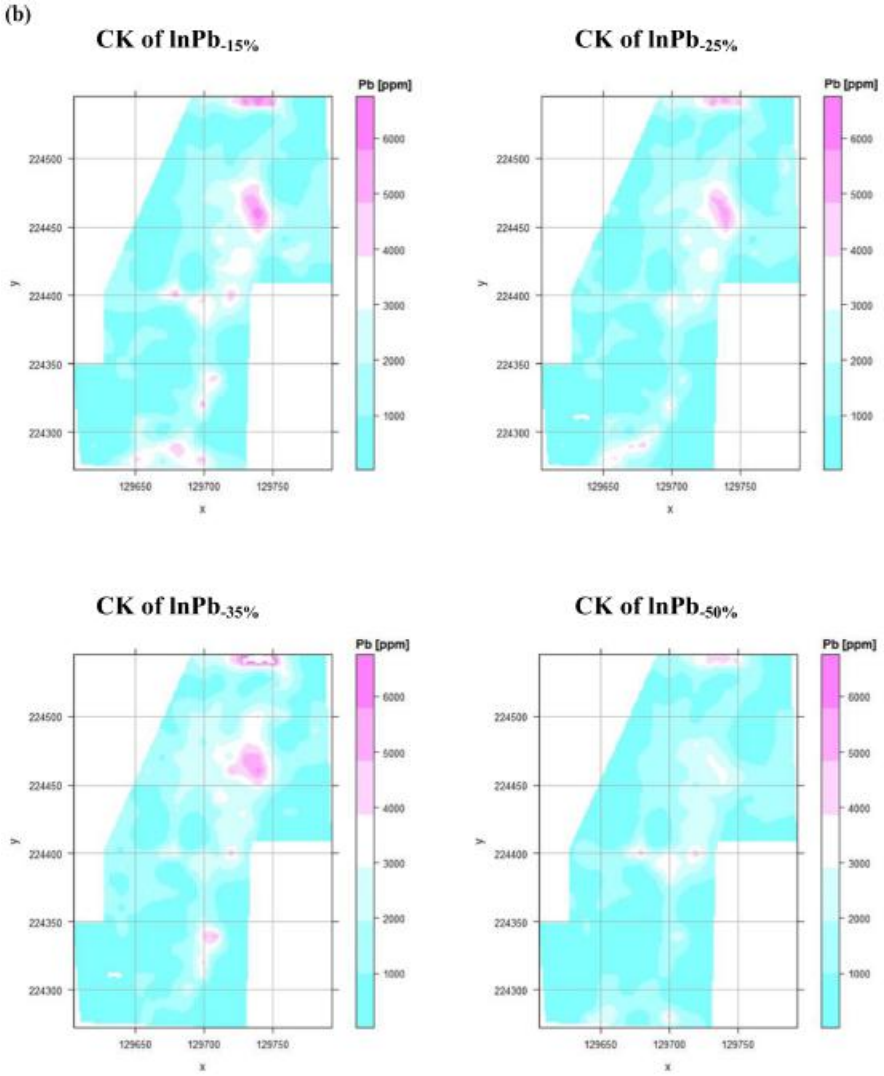

Figure 1. Interpolated maps of Pb generated using a) ordinary kriging and b) ordinary cokriging models. Data was back-transformed prior to creation of contour maps.